

Article

# Dynamics of Permafrost Coasts of Baydaratskaya Bay (Kara Sea) Based on Multi-Temporal Remote Sensing Data

Anna Novikova <sup>1,\*</sup>, Nataliya Belova <sup>1</sup>, Alisa Baranskaya <sup>1</sup> , Daria Aleksyutina <sup>1</sup>, Alexey Maslakov <sup>1</sup>, Egor Zelenin <sup>2</sup>, Natalia Shabanova <sup>1</sup> and Stanislav Ogorodov <sup>1</sup>

<sup>1</sup> Laboratory of Geoecology of the North, Faculty of Geography, Lomonosov Moscow State University, GSP-1, Leninskie Gory, 119991 Moscow, Russia; nataliya-belova@yandex.ru (N.B.);

alisa.baranskaya@yandex.ru (A.B.); aleksyutina@gmail.com (D.A.); alekseymaslakov@yandex.ru (A.M.); nat.volobuyeva@gmail.com (N.S.); ogorodov@aha.ru (S.O.)

<sup>2</sup> Laboratory of Neotectonics and Modern Geodynamics, Geological Institute, Russian Academy of Sciences, Pyzhevsky lane, 7, 119017 Moscow, Russia; egorzelenin@mail.ru

\* Correspondence: annamsu17@gmail.com; Tel.: +7-495-939-2526

Received: 8 August 2018; Accepted: 11 September 2018; Published: 16 September 2018



**Abstract:** Arctic coasts composed of frozen deposits are extremely sensitive to climate change and human impact. They retreat with average rates of 1–2 m per year, depending on climatic and permafrost conditions. In recent decades, retreat rates have shown a tendency to increase. In this paper, we studied the coastal dynamics of two key sites (Ural and Yamal coasts) of Baydaratskaya Bay, Kara Sea, where a gas pipeline had been constructed. Based on multi-temporal aerial and satellite imagery, we identified coastal erosion rates at several time lapses, in natural conditions and under human impact, and discussed their temporal variability. In addition to planimetric (m/yr), we calculated volumetric (m<sup>3</sup>/m/yr) retreat rates of erosional coasts using ArcticDEM. We also estimated the influence of geomorphology, lithology, and permafrost structure of the coasts on spatial variations of their dynamics. Erosional coasts of the Ural key site retreat with higher mean rates (1.2 m/yr and 8.7 m<sup>3</sup>/m/yr) as compared to the Yamal key site (0.3 m/yr and 3.7 m<sup>3</sup>/m/yr) due to their exposure to higher open sea waves, more complex lithology, higher ice content and lower coastal bluffs. Since the 1960s, coastal retreat rates have been growing on both coasts of Baydaratskaya Bay; we relate this effect with Arctic climate warming. From the 1960s to 2005, such growth was moderate, while in 2005–2016 it became rapid, which may be explained by the enhanced wave and thermal action or by the onset of industrial development. The adjacent coastal segments, originally accumulative, remained relatively stable from the 1960s to 2005. After 2005, a considerable part of them began to retreat as a result of changing weather conditions and/or increasing human impact.

**Keywords:** permafrost; coastal erosion; Baydaratskaya Bay; remote sensing

## 1. Introduction

Permafrost coasts make up to 34% of the world's coastlines and retreat with an average rate of 0.5 m/yr [1]. Dynamics of Arctic coasts composed of frozen unlithified sediments have a strong influence on terrestrial [2,3], marine [4,5], and atmospheric [6] systems. In recent decades, coastal erosion accelerated in most of the polar regions due to rapid climate change, with its impact on the Arctic two times larger than on the rest of the world [7,8]. The decline of sea ice extent [9,10], storm frequency increase [11,12], thermal and wave action growth [13], and sea-level rise [14] have a dramatic impact on the arctic coastal dynamics [15–20].

Numerous studies provide detailed data on contemporary coastal dynamics at local [21–23] and regional [24,25] scales. Studies on the Beaufort Sea coast [26,27] and the Chukchi Sea coast of Alaska [28] showed an increase in retreat rates at the beginning of the 21st century. At the same time, little of the Arctic coast is covered by multi-temporal studies. Remoteness and vastness of the polar regions make it difficult to conduct comprehensive field studies on coastal erosion, and therefore, estimate reliable circum-Arctic trends. Application of remote sensing techniques, such as satellite and aerial imagery [29–31], unmanned aerial vehicles (UAVs) [32–34], light detection and ranging (LiDAR) [35] surveys, etc., provides reliable data for observing, quantifying, modeling and monitoring coastal dynamics over vaster regions and larger time periods compared to instrumental measurements.

About 20% of the Kara Sea coasts are thermoerosional [25] (Figure 1). They retreat especially intensively due to their composition of ice-rich permafrost and the presence of ice wedges and massive ice bodies, their thawing is resulting in formation of retrogressive thaw slumps [15,36], thermoerosional niches and gullies [37,38]. Surveys of coastal dynamics in the Kara Sea region at Yugorsky Peninsula [21,39], Baydaratskaya Bay [40–42], and Western Yamal [25,43,44] revealed mean annual coastal erosion rates ranging from 0.5 to 2.5 m/yr, what is significant in comparison to other Arctic regions. Most of these works were based on the results of field monitoring along separate profiles, conducted for two or three decades. The profiles were typically set every 100–500 m. Such low spatial resolution made it challenging to estimate the relative input of different drivers into the resulting retreat rates. To reliably assess rates of coastal erosion and to determine the contribution of various factors, data with higher spatial and temporal resolution are required. Obtaining such data has become much easier in recent decades thanks to high-resolution aerospace imagery.

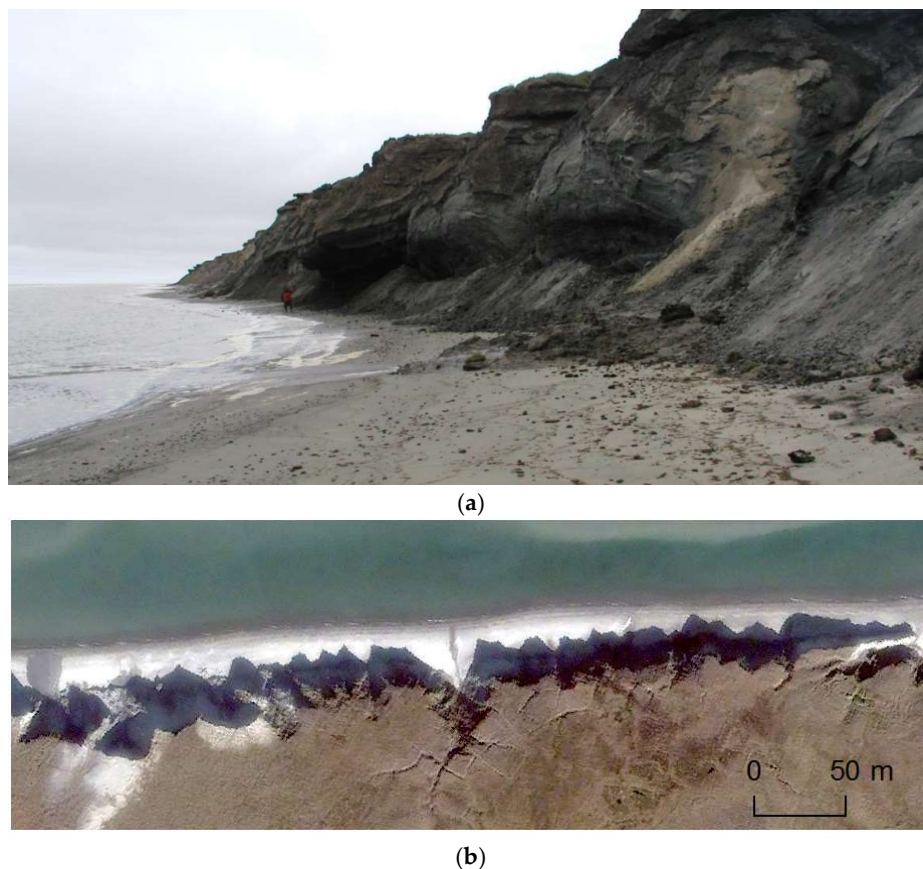


**Figure 1.** Typical thermoerosional coast of the Kara Sea: (a) field view and (b) QuickBird-2 (2005) satellite imagery (natural color composite), the Ural coast of Baydaratskaya Bay.

In the present study we consider the coast as the zone of modern wave action, including foreshores with beach ridges, beaches, coastal bluffs, and low-lying laidas (inundated during the highest tides and storm surges), as well as adjacent areas indirectly influenced by sea wave action (such as thermal gullying, khasyrei formation on the surface of terraces, etc.). We focused on coastline (top of the bluffs on the erosional coasts or dense vegetation boundary on the accumulation coasts) as indicator of shifting of the entire coastal zone.

The present study aims at estimating rates of the coastal changes of Baydaratskaya Bay (Kara Sea) from the 1960s to 2016 using remote sensing accompanied by long-term field monitoring data. The Ural and the Yamal coasts of Baydaratskaya Bay were chosen as key sites because (1) they have different geomorphic and geographic conditions, which allows to estimate their impact on coastal erosion, and (2) the underwater part of the gas pipeline Bovanenkovo-Ukhta crossing Baydaratskaya Bay was built at these two sites in 2009–2012, making it possible to compare natural conditions with the period of human impact. For the first time, the rates of coastal retreat for these study areas were based on the interpretation of series of aerial and satellite imagery from the 1960s until 2016. Besides planimetric, we calculated volumetric rates of coastal retreat, which are more demonstrative, more relevant for coastal erosion modelling, and enable sediment flux calculation [22]. An accuracy of calculated values was estimated. The spatial and temporal variability of retreat rates were analyzed. Analysis of spatial variations of permafrost conditions as well as temporal variations of climatic conditions allowed us to assess the possible human contribution to coastal dynamics.

## 2. Study Area

The Kara Sea is located in the western part of the Eurasian Arctic ocean shelf (Figure 2). Two key sites of the study are located in the western part of the Kara Sea on the western (Ural) and the eastern (Yamal) coasts of Baydaratskaya Bay (Figure 2). The Ural key area is an 11 km long coastal segment between the mouth of the Ngoyuyakha River in the west, and the laida (low surface inundated during the highest tides and storm surges) on the eastern side of the Nyudyako-Tambyaha River in the east (Figure 3). The Yamal key area is a 12.5 km long coastal segment between Cape Mutniy in the north and the ravine 4 km north of the Liyaha River's mouth in the south (Figure 3).

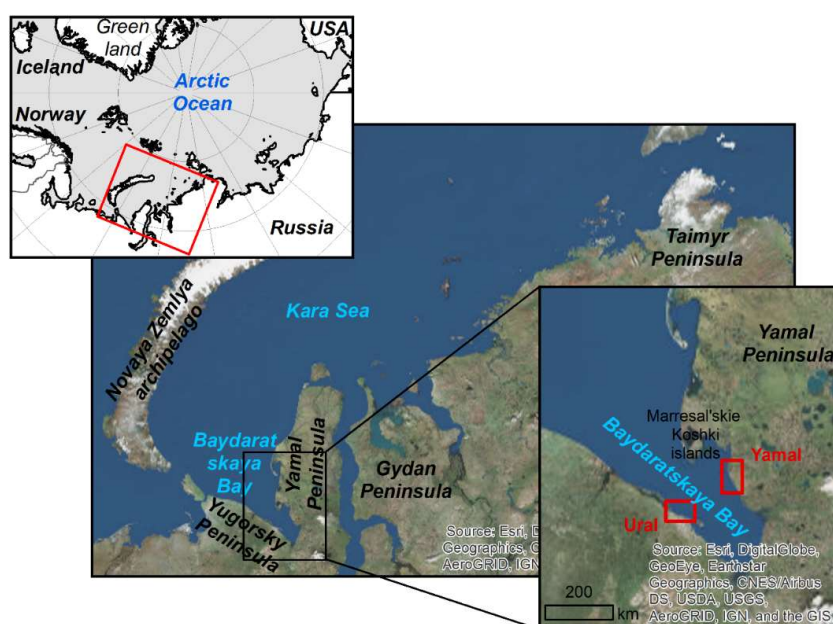


**Figure 2.** Study area. On the inset in the top left corner the red rectangle shows the Kara Sea region. On the inset in the bottom right corner red rectangles show the key sites (Figure 3).

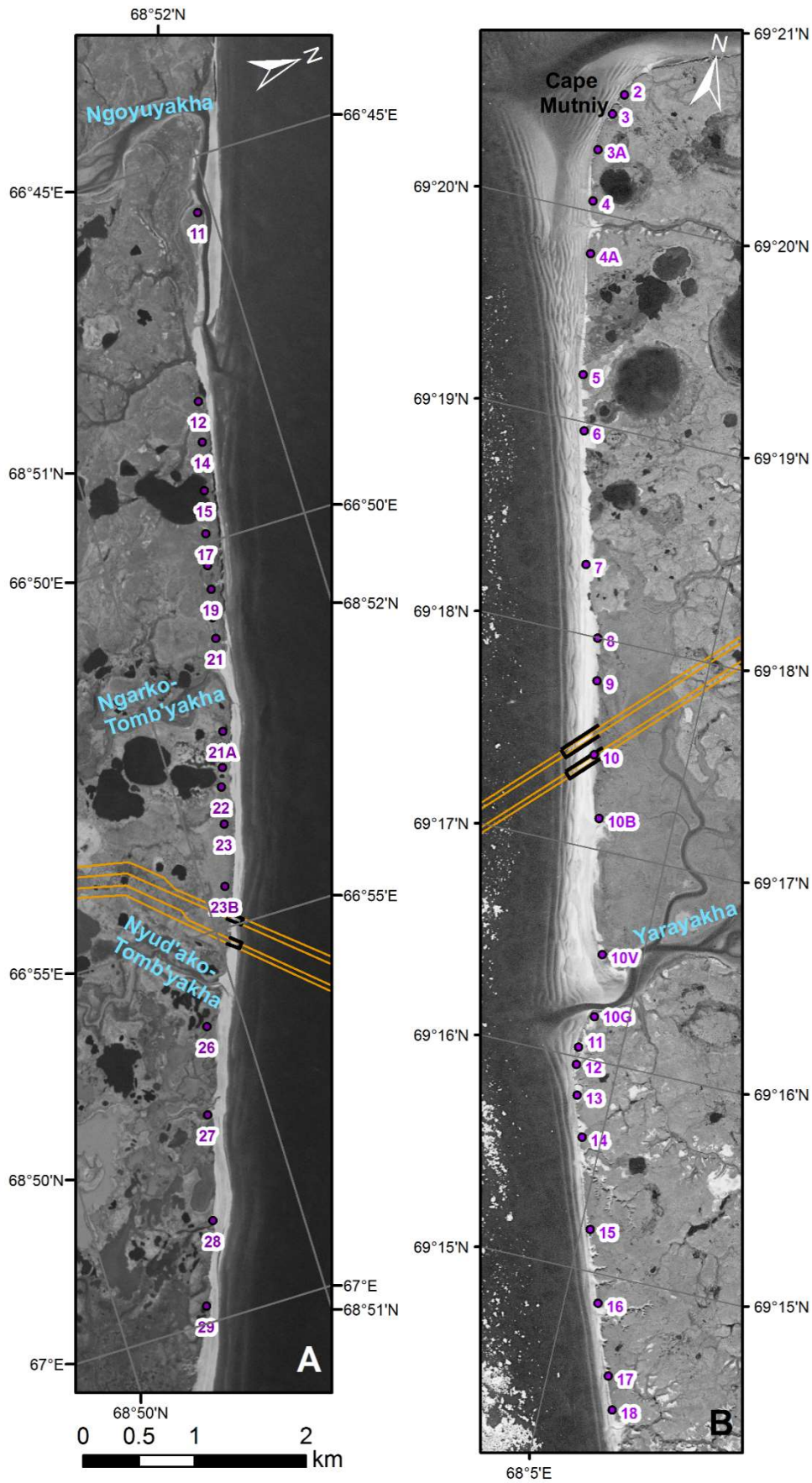


**Figure 3.** Key sites of the study: (A) Ural coast and (B) Yamal coast of Baydaratskaya Bay, the Kara Sea. Orange lines show the gas pipelines; black lines show the cofferdams. Background: (A) Corona KH-4A, 1964, and (B) Corona KH-4A, 1968.

The climate of the region is severe. Average annual air temperatures range from  $-7$  to  $-10$  °C [45]. The cold period (the period with mean daily temperatures below zero) lasts for about 250 days, from October to the middle of June. The amount of annual precipitation is 300–500 mm. Strong winds and storms from the sea are frequent. In winter, the prevailing wind direction is seaward (from the south); in summer, it is directed inland (from the northwest). Inland-directed winds in summer provoke waves that transmit their energy to the coast and erode it during the ice-free period. In the warm period (June–September) the prevailing wind velocity is 3–6 m/s (50% of observations); in the cold period, it is 4–8 m/s (52%). The frequency of strong winds  $>10$  m/s is 10% in summer and 20% in winter. The sea is completely ice-free for only two months (August–September). The maximum value of tide-driven (combined with wind-surges) sea level fluctuations is 0.8–1.0 m [46].

The area is underlain by continuous permafrost, with thickness down to 40–50 m on the Ural coast and down to 50–100 m on the Yamal coast. The mean annual ground temperature at the depth of zero annual amplitudes ranges from  $-2$  to  $-5$  °C. The thickness of the seasonal thawing layer varies from 0.3–0.4 to 2 m [46]. Thermodenudation processes, such as thermokarst, thermal erosion (gulying), frost cracking, and mass movements, are widespread.

The south-western Kara Sea shelf is shallow: its depths do not exceed 100 m. Depths of Baydaratskaya Bay are less than 40 m. The coasts are low swampy plains. Coastal plains at the Ural and Yamal key sites have several levels of topography, relatively similar to each other (Table 1).

**Table 1.** Topography levels at the Ural and Yamal key sites.

Height, m a.s.l.	Landforms	Lithological and Permafrost Composition
<i>Ural Coast</i>		
–9–1	Modern shore	Series of sandy beach ridges at 2–9 m depth, pebbly-sandy tidal flat and sandy beach up to 200 m width, unfrozen
2–4	Holocene laida (2–4 m laida)	Ice-rich loams overlain by peats and sands with pebbles, massive and reticulate cryostructure with wedge ice
6–8	Late Pleistocene low terraces (T6–8 m)	Sands with ice wedges underlain by loams with few pebbles and boulders, massive cryostructure
12–16, up to 20	Late Pleistocene [47] high terrace (T12–16 m)	Thin laminated sands, with multiple massive ice beds, ice lenses and wedge ice outcrops in coastal bluffs [48]. Exposed massive ice beds reach 3.5 m vertically and 80 m laterally. Drained lake basins are widespread.
<i>Yamal Coast</i>		
–9–1	Modern shore	Series of sandy beach ridges at 2–9 m depth, a tidal flat composed of thin sands and beach of sands with sparse pebbles up to 150 m in width, unfrozen
2–4	Holocene laida	Sands with pebble underlain by loams, extending to the Yarayakha River valley, and divided from the sea by a sandy barrier beach, mostly unfrozen
6–8	Late Pleistocene terraces (T6–8 m)	Sands, massive cryostructure
12–16	Late Pleistocene [49] terrace (T12–16 m)	Sands in the north of the study area near Cape Mutniy and pebbly loams in the southern part of the study area on the left side of Yarayakha, which could be correlated to the so-called Kara Diamicton of the Marresale area [50–52], and are either of glacial or marine origin. Massive and reticulate cryostructure
25–30	Late Pleistocene terrace (T25–30 m)	Thin laminated sands with clays at the base of the bluff. The sediments have low ice content; a few ice lenses in sands and wedge ice in peat was reported [51]. Sandy strata are supposed to correlate to Oleniy and Baidarata sands at the Marresale area [50–52]

In 2009–2012, the underwater crossing of Baydaratskaya Bay by the gas pipeline Bovanenkovo-Ukhta was built. Two cofferdams, buildings, and roads were constructed at each key site; some dredging was done at the mouth of the Yarayakha River; sediments were excavated from the beach. Human impact also included heavy vehicles driving on the surfaces of low terraces, laidas, beaches, and tidal flats [42].

### 3. Materials and Methods

#### 3.1. Remote Sensing Data

The rates of coastal advance/retreat at Baydaratskaya Bay reach up to a few meters per year [42]. Remote analysis of these dynamics demands high spatial resolution remote sensing data, its proper correction, and precise georeferencing. In this study, we used Corona KH-4, QuickBird-2, WorldView-2, and WorldView-3 optical space-borne and aerial imagery with spatial resolution from 7.5 to 0.3 m (Table 2). We considered the dynamics of the two key sites of the Kara Sea for the whole period of study: 1964–2016 for the Ural site and 1968–2016 for the Yamal site, as well as for different periods: 1964–1988, 1988–2005, 2005–2012, and 2012–2016 for the Ural site and 1968–1988, 1988–2005 and 2005–2016 for the Yamal site, respectively (Figures in the Section 4). During long-term time lapses (from the 1960s to 2005), we observed natural coasts that were undisturbed by human development, whereas the recent short-term time lapses (from 2005 to 2016) included the period of pipeline construction (2009–2013), which was supposed to influence the coastal dynamics.

To determine the position of the coastline in the 20th century, Corona satellite imagery and aerial imagery were used. Corona is declassified military satellite imagery from 1960–1972 with global coverage and the highest ground resolution of up to 1.8 m. It is distributed by the U.S. Geological Survey [53] as scanned film strips 70 mm × 75.6 cm in size in four image tiles with a 7 µm (3600 dpi) scan resolution. Due to its large elongated coverage, Corona images are strongly affected by perspective distortions, especially on the margins [30,54]. Our study areas did not exceed 50 km<sup>2</sup> and are both located in the center of the film strips. Therefore, we did not undertake geometric correction of the whole strip. The part of the image covering key areas was referenced to the modern images with a spline transformation. Aerial imagery was acquired as analogue photographs with an 18×18 cm frame size and was scanned at a 40 µm (600 dpi) resolution.

**Table 2.** Remote sensing data for the Ural and Yamal key sites.

Sensor	Date	Resolution (m)	RMSE of Coregistration (m)	Topography-Induced Uncertainty (m)	Processing Level
<i>Ural coast</i>					
Corona KH-4A	09.08.1964	7.5	7	-	Raw
Aerial	10.07.1988	0.7	0.8	-	Raw
QuickBird-2	31.08.2005	0.6	1.1	3.2	Ortho Ready Standard
WorldView-1	22.07.2012	0.5	0.2	4.9	Ortho Ready Standard
WorldView-2	31.07.2013	0.5	0.3	4.9	Ortho Ready Standard
WorldView-2	21.05.2016	0.5	0.8	5.9	Standard
<i>Yamal coast</i>					
Corona KH-4	21.08.1968	2	8	-	Raw
Aerial	10.07.1988	0.7	1.1	-	Raw
QuickBird-2	29.08.2005	0.5	0.6	6.6	Standard
WorldView-3	21.06.2016	0.3	0.4	3.8	Standard

For the 21st century (2005–2016), Digital Globe products (QuickBird and WorldView images) were used. They were provided as digital scenes with full metadata. Digital Globe products had the geolocation accuracy of 23 m CE90 for the QuickBird imagery and 5 m CE90 for the WorldView imagery.

The imagery we analyzed initially had the following levels of processing:

- **Raw images** (Corona and aerial imagery): unprocessed. The metadata of Corona contained the entity ID (mission and frame numbers), acquisition date, camera type (aft/forward/cartographic/vertical), and camera resolution (stereo medium/stereo high/vertical low/vertical medium/vertical high). The metadata of aerial imagery implied flight and frame numbers, and acquisition date.

- **Standard** (WV2 2016 for Ural, WV3 2016 for and QB2 2005 for Yamal): the imagery was radiometrically corrected, sensor corrected, and map projected, normalized for topographic relief with respect to the reference ellipsoid applying a coarse DEM.
- **Ortho Ready Standard** (QB2 2005, WV1 2012 and WV2 2013 for Ural): the imagery was radiometrically corrected, sensor corrected, and map projected, had no topographic relief being applied with respect to the reference ellipsoid, making it suitable for orthorectification.

All chosen imageries were acquired from the end of May to mid-October when the water area was ice-free and the coastal bluff was not covered with snow.

Therefore, the imagery had a resolution appropriate to study coastal dynamics, but it required geometric correction (orthorectification) and thorough georeferencing before measuring coastal erosion/accretion rates.

### 3.2. Fieldwork

The Laboratory of Geoecology of the North, MSU, in cooperation with Zubov State Oceanographic Institute, carried out monitoring of coastal dynamics of the key areas since the 1980s. During numerous expeditions, recurrent (almost every summer) topographic surveys along a network of profiles (Figures 3 and 5) were conducted. The surveys started as direct measurements by tape; in the last decades, they were executed by a LEICA TCR802 or SOKKIA SET 230 RK3 total station. Last year, we combined tachymetric surveys around the gas pipelines with DGPS through a Javad Sigma G3T DGPS receiver both in RTK and in static modes along the profiles of the coastal monitoring network. The morphology, lithology, and permafrost of key areas as factors of coastal dynamics were mapped and described.

Application of the field data was restricted since it was collected during expeditions of the private company and the most of original data is not allowed for open publication. The present study was based on the remotely sensed data primarily. Among the field data, we used exclusively (1) DGPS GCPs for imagery referencing, (2) data on morphology, lithology, and permafrost conditions collected in field, and (3) mean rates calculated as a result of topography surveys along the profiles of monitoring to control our results.

### 3.3. Georeferencing and Orthorectification

The first step was referencing the 2016 WorldView images to a network of differential GPS (DGPS) ground control points (GCPs), which were collected during fieldwork in summer 2016, by a first-order polynomial (affine) transformation. The original geolocation accuracy of these images was claimed to be 5 m; as DGPS accuracy comprised a few cm, it was enhanced to 0.4–0.8 m. Creating a network of GCPs in tundra landscapes was challenging due to the paucity of well-identifiable stable features, such as man-made infrastructure in unsteady permafrost landscapes. Our DGPS GCPs network included buildings, cofferdams, pipelines, and roads in the center of the key sites. Earlier images were referenced to 2016 WV2 by a second-order polynomial with a large quantity of natural control points: small lakes, forelands of lakes' shoreline, and corners of permafrost polygons. KH-4 Corona images were referenced by splines with as many control points as possible.

The studied territory is relatively flat with height differences of less than 30 m. Heights of coastal cliffs do not exceed 16 m at the Ural coast and 20 m at the Yamal coast. Through Equation (1), we calculated the uncertainty of relief-induced horizontal displacement ( $\delta_t$ ) (in case of necessary data provided with the imagery):

$$\delta_t = \operatorname{tg}\alpha \times h, \quad (1)$$

where  $\alpha$  is the tilt angle of the spacecraft and  $h$  is the maximum relative height at the territory. The uncertainty varied from 3.2 to 6.6 m depending on the topography and tilt angle of the space imagery acquisition (Table 2).

To reduce topography-induced distortions, we conducted orthorectification, where it was possible. We created orthomosaics from aerial photographs of 1988 using Agisoft PhotoScan Pro 1.4. We carried

out orthorectification of the WV-2 2013 image of the Ural coast and the WV-2 2016 image of the Yamal coast applying freely distributed ArcticDEM ([55], 5 m spatial resolution and 0.3 m vertical accuracy, according to [56]) in ArcGIS 10.2 (ESRI). Possibly due to flat relief, the differences we revealed were negligible (up to 1 m) and appeared around the cliff bottom only, i.e., the position of the cliff top did not change after orthorectification. The offset between the standard product (orthorectified while using coarse DEM by the provider) and manually-rectified imagery was barely visible as well.

All the images were projected using the respective UTM zone (42N) on a WGS-84 datum.

#### 3.4. Coastline Tracing and Quantitative Assessment of Coastal Dynamics

We traced the coastline along the top of the cliff at erosional sections and along the dense vegetation boundary (upper limit of high waves action) at accumulative sections. In some cases, tracing the coastline on aerospace images, and even in the field, was challenging and argued. For instance, in the study areas the cliff-top of the low-lying coastal plains was often buried by aeolian sands (Figure 4A) or the dense vegetation boundary was unclear and gradual (Figure 4B). Tracing the shoreline at such sectors was especially complicated, often impossible, on the bleached analogue aerial or Corona images of lower resolution. On the large sectors of pipeline and other infrastructure construction, the shoreline was substantially disturbed.

As the principal aim of the study was the analysis of coastal dynamics in permafrost conditions, we mainly focused on erosional segments composed of frozen deposits (while sandy spits, barrier beaches, and low-lying laidas of the accumulative segments are commonly unfrozen). Moreover, at the erosional segments the cliff-top as shoreline was definitely identifiable and had a clear unidirectional tendency to retreat, what made a detailed quantitative assessment of coastal dynamics possible here. Owing to foresaid, we accomplished quantitative transects analysis for these segments. However, adjacent accumulative segments were analyzed as well in order to obtain an integrative view of the process. For these segments, we provided a qualitative assessment with rates' estimation for separate sections, where possible.

We digitized coastline manually using ArcGIS 10.2 (ESRI Inc., Redlands, CA, USA) software at pixel accuracy equivalent to scales from 1:300 to 1:2000. To calculate the shoreline position changes, we used the Digital Shoreline Analysis System (DSAS) of Thieler et al. [57], available as an extension to ArcGIS. The program automatically creates transects normal to the general direction of the shorelines (baseline) with an optional spacing along the baseline. Then, it measures the coastal retreat rates as an offset from the baseline  $L(t_i)$  for imagery acquisition dates  $t_i$ , and calculates statistics on the overall retreat rates and their uncertainty. As coastal features and lithological units extended for hundreds of meters along the coast (see figures in the Section 4), we considered 200 m as the lowest limit of spacing that provides consistent results. However, we arbitrarily assigned the spacing value to 50 m to ensure the visually continual set of transects for further analysis. We built transects for erosional segments of the coasts: 117 on the Ural and 128 on the Yamal. Transects crossing rivers and gullies, and areas of undefined coastline position were omitted from statistics calculation (20 on the Ural coast and 9 on the Yamal coast).

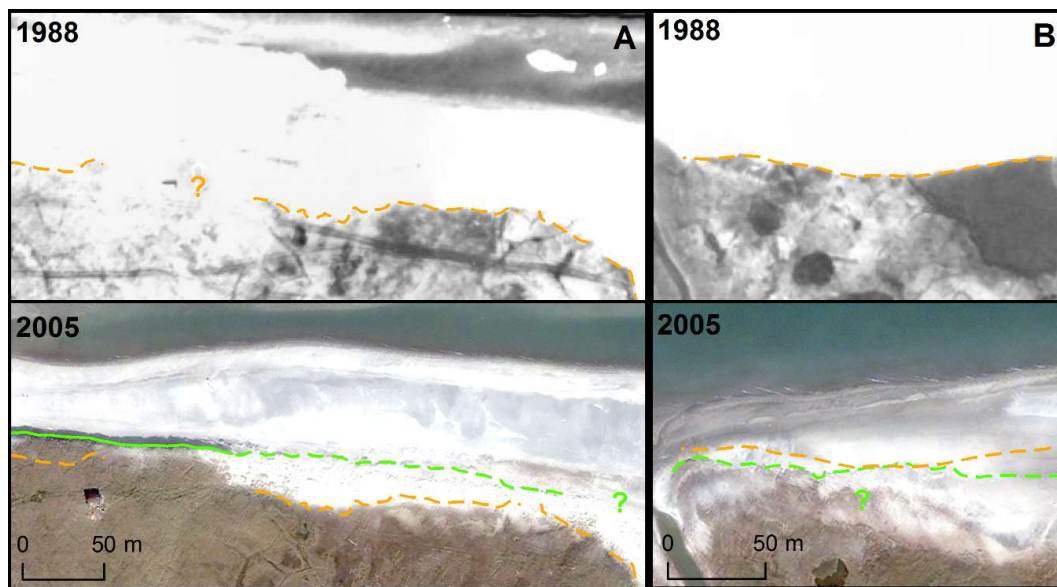


**Figure 4.** Sectors of the Ural coast where shoreline tracing is complicated due to (A) aeolian sandy cover on top of the marine terrace, and (B) diffuse dense vegetation boundary: aerial image (above); QuickBird2 image (below).

After digitalization, we calculated the retreat rates for each time span between imagery acquisitions in m/yr:

$$r_L(\tau_{i-1}, \tau_i) = \Delta L / \Delta \tau = (L(t_i) - L(t_{i-1})) / (t_i - t_{i-1}), \quad (2)$$

assuming  $r_L > 0$  for progradation and  $r_L < 0$  for retreat of the coast.

This parameter shows the velocity of the coastline movements in the plan (planimetric or linear), crucial for engineering. However, studies of sediment balance require knowledge of the amount of deposits that were eroded and accumulated. The volume of the eroded deposits can be assessed based on the obtained values of shoreline retreat ( $r_L$ ) and the altitudes of transections extracted from ArcticDEM ( $h$ ) in cubic meters from one meter of shoreline (Figure 5):

$$r_V = h \times r_L. \quad (3)$$

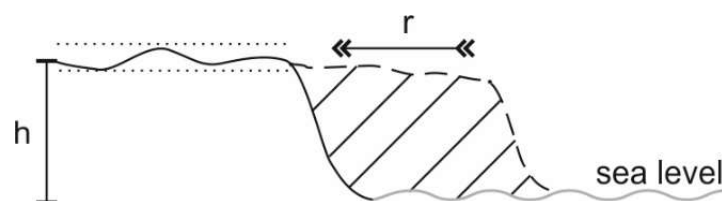


**Figure 5.** Schematic transect across the cliff. The eroded area (dashed) is a product of cliff height ( $h$ ) and linear retreat ( $r$ ). The accuracy of this value relies on the uncertainty of retreat and variations of the eroded surface height assumed to be similar to variations of the modern surface height.

We classified coastline transects depending on their geomorphologic, lithologic, and permafrost conditions to reveal the impact of these conditions on spatial variations of coastal dynamics (Table 1).

### 3.5. Uncertainty Assessment

The accuracy of the coastline position was estimated by adapting the method of Günther et al. [30]. The following sources of uncertainties were taken into consideration:

1. spatial resolution of the imagery ( $\delta_s$ );
2. relative georeferencing of two datasets to each other ( $\delta_r$ ); and,
3. topography-induced horizontal displacement ( $\delta_{ot}$ ,  $\delta_t$ ,  $\delta_{at}$ ).

The first uncertainty  $\delta_s$  is an arbitrary set value of how accurate the coastline could be digitized on a raster. For all of the remote sensing data it was assigned to be one half of the imagery spatial resolution as provided by an imagery distributor. Coasts where such accuracy was unfeasible were excluded from measurements. The uncertainty  $\delta_r$  of the imagery georeferencing was obtained as the total RMS (root mean square) error in the link table, which was the geometric mean of mismatch of individual links to the referenced image.

The relief-induced error was calculated as:

$$\delta_{ot} = \Delta z \operatorname{tg} \alpha, \quad (4)$$

where  $\alpha$  is the tilt angle of the spacecraft and  $\Delta z$  is the vertical accuracy of the DEM using for orthorectification. A straightforward method of estimating the vertical accuracy is to consider it equal to the variation of the sea surface height at the cliff bottom, which comprised  $\Delta z = 0.2$  m. As a virtually flat surface of the sea was located just at the studied coastline, the accuracy of the DEM was clearly visible as both high-frequency noise and gradual offsets. However, for earlier imagery, no DEM was suitable, so we considered the eroded surface to be at the same height as the modern cliff, and derived the topographic-induced uncertainty  $\delta_t$  from the topography amplitude at the cliff (1) instead of the vertical accuracy.

Aerial imagery had overlapping coverage for the entire area, sufficient to build a three-dimensional (3D) model and an orthomosaic. As we had no reliable GCPs at that time, we built the orthomosaic in local coordinates with no prior parameters except the focal length  $f = 200$  mm and the frame size  $s = 18$  cm, and subsequently co-registered the whole orthomosaic. The automatically-constructed model kept the sea surface flat and horizontal, so the main source of error was a high frequency noise, not exceeding  $dz = 2$  m, which might cause a horizontal offset of not more than:

$$\delta_{at} = dz \operatorname{tg} a = dz s / 2f, \quad (5)$$

The oldest available imagery for the study area was KH-4A Corona scanned films. As no acquisition geometry was known and the films were occasionally distorted [30,54], we preferred to co-register the raster using a spline function with tie points only in the neighborhood of the study areas. Here, the best estimation of accuracy was the RMSE of the control points offset at the co-registration.

All of the mentioned error sources resulted in an overall error as independent sources:

$$\delta_x = \sqrt{\delta_{ot}^2 + \delta_r^2 + \delta_s^2}, \quad (6)$$

for orthorectified imagery,

$$\delta_x = \sqrt{\delta_t^2 + \delta_r^2 + \delta_s^2}, \quad (7)$$

for non-rectified imagery,

$$\delta_x = \sqrt{\delta_{at}^2 + \delta_r^2 + \delta_s^2}, \quad (8)$$

for aerial imagery,

$$\delta_x = \sqrt{\delta_r^2 + \delta_s^2} \quad (9)$$

for KH-4 Corona.

The total uncertainty of the rate of the changing coastline position from  $x_1$  to  $x_2$  during the period from  $t_1$  to  $t_2$  was calculated as:

$$\delta_r = \frac{\sqrt{\delta x_1^2 + \delta x_2^2}}{t_1 - t_2} \quad (10)$$

The volumetric approach uses heights of eroded surface as well as rates of planar retreat, so the total uncertainty of volumetric rates  $\delta_{rV}$  comprised:

$$\delta_{rV} = \sqrt{h^2 \delta_r^2 + r^2 \delta_h^2} \quad (11)$$

where  $\delta_h$  is an accuracy of estimation of the eroded surface height, depending on the surface roughness and equal to the height variance of the eroded surface at the current cliff.

### 3.6. Hydrometeorological Stress Calculation

The temporal variability of erosion rates in natural conditions in permafrost areas depends on a combination of two main factors, enhancing each other: the thermal and the wind-wave energy conditions. The thermal factor is determined by positive air temperatures, providing the thawing of permafrost in coastal bluffs. The wind-wave energy depends on the ice-free period duration, length of the wave fetch, sea depth, and wind velocity [42]. It controls how fast the thawed material is removed by waves; calculating its changes is therefore, important for the understanding of coastal retreat mechanisms in the Arctic regions [11,24,26,58]. With ongoing climate warming, both air temperature and wind-wave energy increase; however, their changes are not simultaneous and they do not always directly relate to coastal erosion rates [25].

The thermal potential of thermodenudation was estimated by the air thawing index showing the number of positive Celsius degree-days per year. A similar parameter called degree days thawing was used in [58]. The ERA-Interim [59] reanalysis was used. Previous studies showed [13] that the reanalysis-derived absolute values could not be used without validation to observation data and removing the systematic error, which might reach 12–20% of the mean value. As far as there are no regular observations at the Yamal and Ural coasts, we used the anomalies (deviations from the long-term 1979–2017 mean) and did not appeal to absolute values.

To calculate the wind-wave energy flux, we applied the Popov-Sovershaev method, which is based on the dependence of the energy flux on ice-free period duration, wave fetch along the wave-dangerous wind direction, wave-dangerous wind direction frequency, and wind speed in third degree [42]. For wind characteristics, we used ERA-Interim data [59]. The ice-free period duration was estimated using OSI SAF daily sea ice concentration data in 12.5 km resolution net of © (2018) EUMETSAT [60]. Wave fetch and wave-dangerous wind directions were derived from ETOPO-1 digital elevation model [61].

The total hydrometeorological influence on coastal dynamics was roughly bounded by a sum of air thawing index and wave energy flux anomalies normalized by standard deviation [13].

## 4. Results

### 4.1. Dynamics of the Ural Coast of Baydaratskaya Bay

About 40% (4.5 km) of coasts of the Ural key site are erosional; they retreat more intensively compared to erosional coasts of the Yamal key site (Tables 3 and 4, Figure 6). Mean retreat rates of the Ural coast (1964–2016) reached  $1.2 \pm 0.15$  m/yr (planimetric, Table 3) or  $8.6 \pm 1.4$  m<sup>3</sup>/m/yr (volumetric, Table 4). Accumulative coasts covering about 60% (6.5 km) of the Ural key site experienced significant changes as well, mostly towards the tendency of retreat.

**Table 3.** Calculated planimetric rates of retreat on the Ural coast (m/yr).

FactorPeriod		1964–1988	1988–2005	2005–2012	2012–2016	1964–2016
Rate Uncertainty		0.3	0.2	0.45	0.3	0.15
landforms	2–4 m laida	1.8	0.2	7.0	0.6	1.7
	T6–8 m	0.9	0.9	3.7	0.9	1.3
	T12–16 m	1.3	1.3	1.0	0.0	1.1
lithology	sands	1.4	1.2	0.8	0.0	1.1
	loams	0.9	1.0	3.7	0.9	1.3
	sands and loams	1.1	1.1	2.6	0.4	1.3
permafrost	massive ice beds	1.1	1.0	2.6	0.5	1.2
	wedge ice	1.2	1.0	2.7	0.4	1.2
mean		1.1	1.1	2.6	0.5	1.2

**Table 4.** Calculated volumetric rates of retreat on the Ural coast ( $m^3/m/yr$ )  $\pm$  rate uncertainty.

FactorPeriod		1964–1988	1988–2005	2005–2012	2012–2016	1964–2016
landforms	2–4 m laida	3.2 $\pm$ 1.0	0.4 $\pm$ 0.6	15.7 $\pm$ 1.9	1.3 $\pm$ 0.9	4.2 $\pm$ 0.6
	T6–8 m	3.2 $\pm$ 2.1	5.8 $\pm$ 1.4	13.5 $\pm$ 3.2	5.2 $\pm$ 2.11	5.8 $\pm$ 1.1
	T12–16 m	12.8 $\pm$ 4.2	13.6 $\pm$ 2.8	8.9 $\pm$ 6.3	0.2 $\pm$ 4.2	12.3 $\pm$ 2.1
lithology	sands	14.1	14.7	9.5	0.3	13.4
	loams	3.3	5.9	13.4	5.5	5.9
	sands and loams	7.6	9.4	11.7	2.1	8.8
permafrost	massive ice beds	7.6	9.4	11.9	3.0	8.9
	wedge ice	7.8	9.0	11.8	2.0	8.7
mean for the study area		7.4	9.2	11.7	2.9	8.7 $\pm$ 1.4

#### 4.1.1. Erosional Coasts

The highest planimetric rates of retreat (up to 2.5 m/yr) were observed within the laida around the Ngarko-Tomb'yakha River (profiles 21A–22, Figure 6). Due to coastal retreat, three lakes up to 100 m in diameter were drained between 1988 and 2005. The smallest retreat (0.2–0.3 m/yr) outside accumulative sectors was noted at the section of the low (6–8 m) terrace directly adjacent to the pipelines from the west (profile 23B) and gradually descending to an accumulative coast towards the east. Generally, high terraces (12–18 m in height) had slower planimetric retreat rates than low terraces (6–8 m in height) and laidas (2–4 m in height): 1.1 m/yr on average, as compared to 1.3 and 1.7 m/yr, accordingly. However, low and high terraces retreated faster than laidas in all periods except 2005–2012, when the dramatic average retreat rates of 7.0 m/yr were observed at laidas, significantly increasing the mean retreat rates over the whole period of 1964–2016 (Figure 7).

The greatest volume of sediment (20–35  $m^3/m/yr$ ) was eroded from the high (12–18 m) terrace between profiles 16 and 19, where the largest massive ice beds outcropped. The retreat of high terraces induced drainage of the very large (up to 620 m in diameter) Zayachie Lake (between 15 and 16 profiles) between 1964 and 1988. The smallest volume was eroded from the laida near the Ngarko-Tomb'yakha River at profiles 21B–22. From 1964 to 2005, more material was washed off from high terraces compared to low terraces (14.1–14.7 and 12.8–13.6  $m^3/m/yr$ , accordingly). From 2005 to 2016, the situation changed, and more sediment was eroded from low terraces (13.5  $m^3/m/yr$  from 2005 to 2012 and 5.2  $m^3/m/yr$  from 2013 to 2016 for low terraces compared to 8.9  $m^3/m/yr$  from 2005 to 2012 and 0.2  $m^3/m/yr$  from 2013 to 2016 for high terraces). The laidas, typically characterized by small volumes of eroded material because of their low surface (from 0.4 to 3.2  $m^3/m/yr$  from 1964 to 2005), experienced enhanced erosion from 2005 to 2013 (up to 15.7  $m^3/m/yr$ ). Volumes washed off from 2012 to 2016 still remained higher in comparison with the high terraces (1.3  $m^3/m/yr$  for laidas, as compared to 0.2  $m^3/m/yr$  for high terraces).

The intensity of coastal erosion in the whole study area varied significantly with time: from 1964 to 2005, both planimetric (1.1 m/yr) and volumetric (from 7.3 to 9.1 m<sup>3</sup>/m/yr) average retreat rates were relatively low. From 2005 to 2013, they both experienced a rapid rise (2.6 m/yr and 11.6 m<sup>3</sup>/m/yr, accordingly). From 2013 to 2016, erosion rates dropped back to values several times less than the background (0.5 m/yr or 2.9 m<sup>3</sup>/m/yr, accordingly).

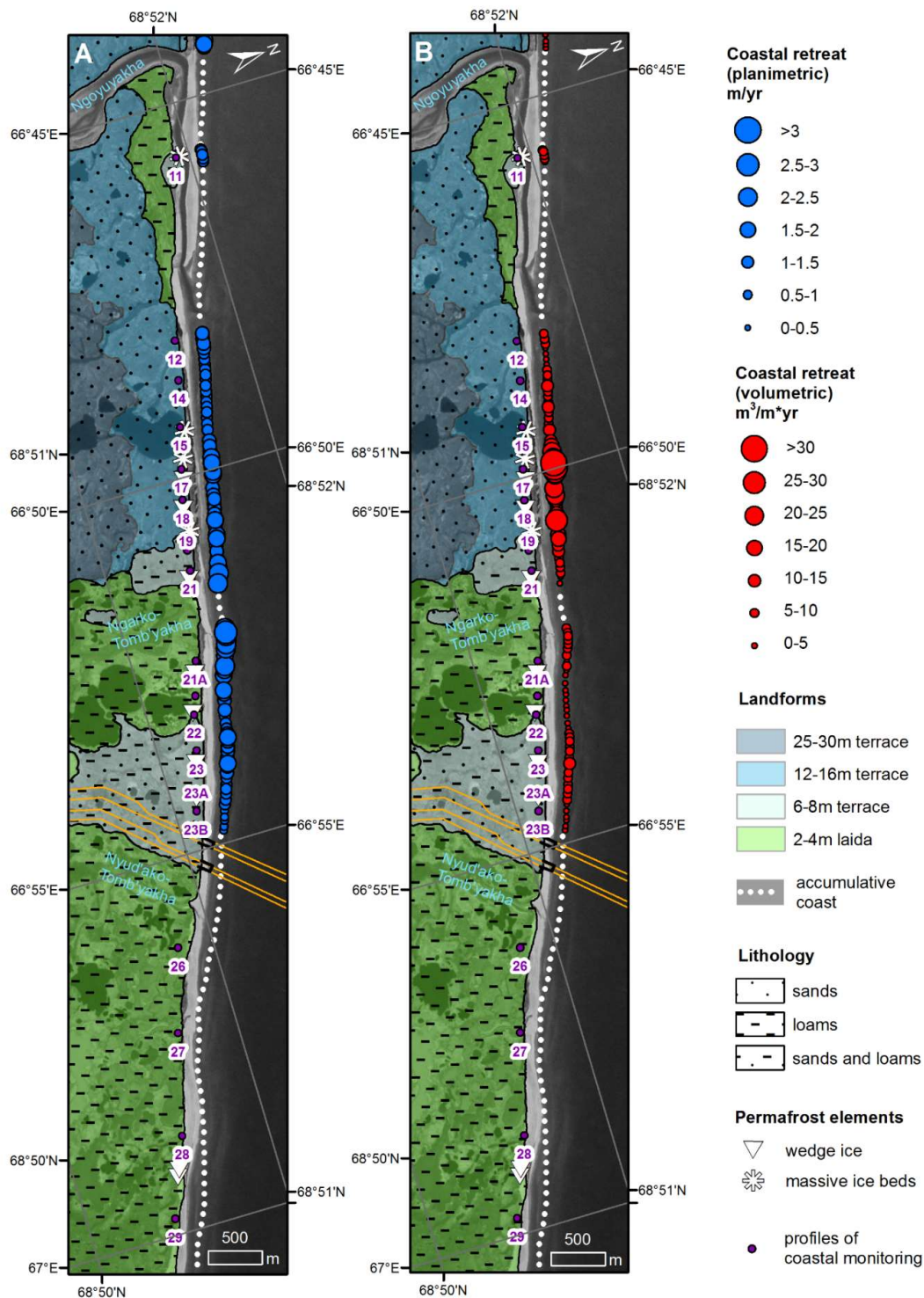


**Figure 6.** Coastal retreat at the Ural key site: (A) planimetric, and (B) volumetric. Orange lines show the gas pipelines; black lines show the cofferdams. Background: Corona KH-4A (1964).

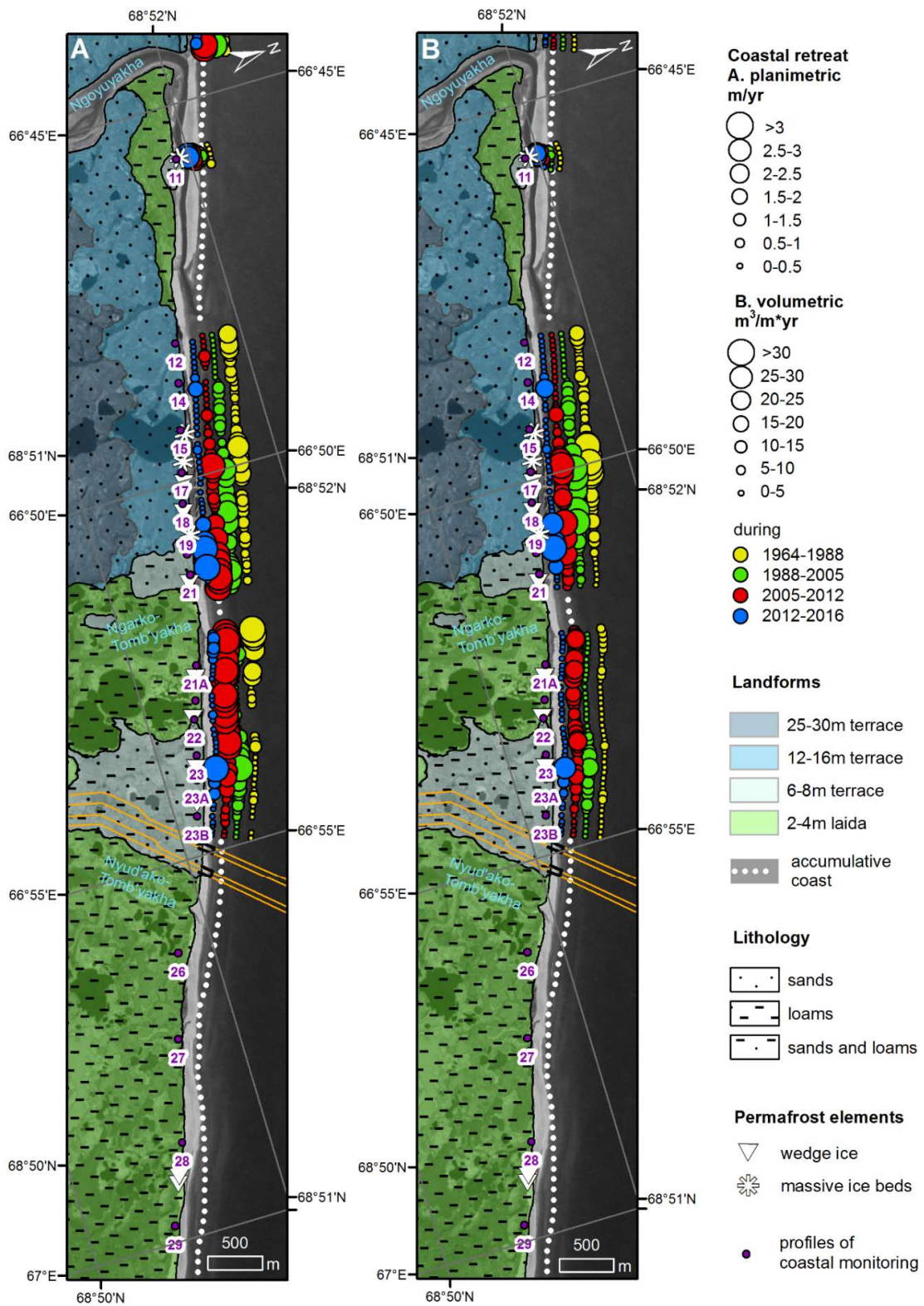


**Figure 7.** Coastal retreat during different periods at the Ural key site: (A) planimetric, and (B) volumetric. Orange lines show the gas pipelines; black lines show the cofferdams. Background: Corona KH-4A (1964).

#### 4.1.2. Accumulative Coasts

The greatest deformations of the accumulative coasts of the Ural key site were observed in its western part, where a sandy spit in the mouth of the Ngoyuyakha River, reaching up to 2 km in length in 1964 was almost completely eroded by the river by 1988. The sediments were transported to the east by a longshore current; and, by 2005, they formed a wide barrier, while a new spit started growing in the river mouth.

The accumulative coast adjacent to the wide laida to the east of the Nyd'ako-Tomb'yakha River remained relatively stable during the observational period; the shoreline moved back and forth (Figure 8). However, the tendency to retreat could be noted on some sections. The coastline near profiles 26 and 27 was degrading since the 1980s: the beach width decreased from 120 m to 40 m, and the dense vegetation boundary moved up to 85 m landward (Figure 8). The beach to the east of the cofferdams also anomalously retreated by 80 m during the period of 2005–2012. Near profile 27, besides the shift of the vegetation boundary, the top of the small bluff retreated up to 80 m landward from 2005 to 2012, making planimetric erosion rates up to 10 m/yr.

#### 4.2. Dynamics of the Yamal Coast of Baydaratskaya Bay

About 62% (7.7 km) of the Yamal key site were erosional during the observational period; however, coastal erosion here was relatively weak: its mean rate for 1968–2016 was  $0.3 \pm 0.16$  m/yr (linear, Table 5, Figure 9A) or  $3.7 \pm 2.1$  m<sup>3</sup>/m/yr (volumetric, Table 6, Figure 9B). Nevertheless, at some sections, changes were considerable, especially at accumulative segments, which represent 48% of the Yamal key site (4.8 km long).

**Table 5.** Calculated planimetric rates of retreat on the Yamal coast (m/yr).

FactorPeriod		1968–1988	1988–2005	2005–2016	1968–2016
rate uncertainty		0.37	0.2	0.38	0.16
landforms	T6–8 m	0.2	0.1	0.9	0.3
	T12–16 m	0.1	0.3	0.5	0.3
	T25–30 m	0.2	0.3	0.6	0.3
lithology	sands	0.1	0.2	0.7	0.3
	loams	0.1	0.4	0.3	0.3
	sands and loams	0.0	0.0	2.2	0.5
permafrost	wedge ice	0.2	0.3	0.5	0.3
mean		0.1	0.2	0.6	0.3

**Table 6.** Calculated volumetric rates of retreat on the Yamal coast (m<sup>3</sup>/m/yr)  $\pm$  rate uncertainty.

FactorPeriod		1968–1988	1988–2005	2005–2016	1968–2016
landforms	T6–8 m	$0.6 \pm 2.6$	$0.7 \pm 1.9$	$3.5 \pm 2.6$	$1.3 \pm 1.2$
	T12–16 m	$2.0 \pm 5.2$	$4.6 \pm 2.9$	$7.7 \pm 5.3$	$4.8 \pm 2.3$
	T25–30 m	$3.3 \pm 10.0$	$6.2 \pm 5.4$	$10.8 \pm 10.2$	$6.4 \pm 4.3$
lithology	sands	1.6	3.1	7.2	3.8
	loams	1.4	4.6	3.3	3.6
	sands and loams	0.1	0.1	7.9	1.8
permafrost	wedge ice	2.8	5.8	9.1	5.7
mean		1.5	3.4	6.4	$3.7 \pm 2.1$

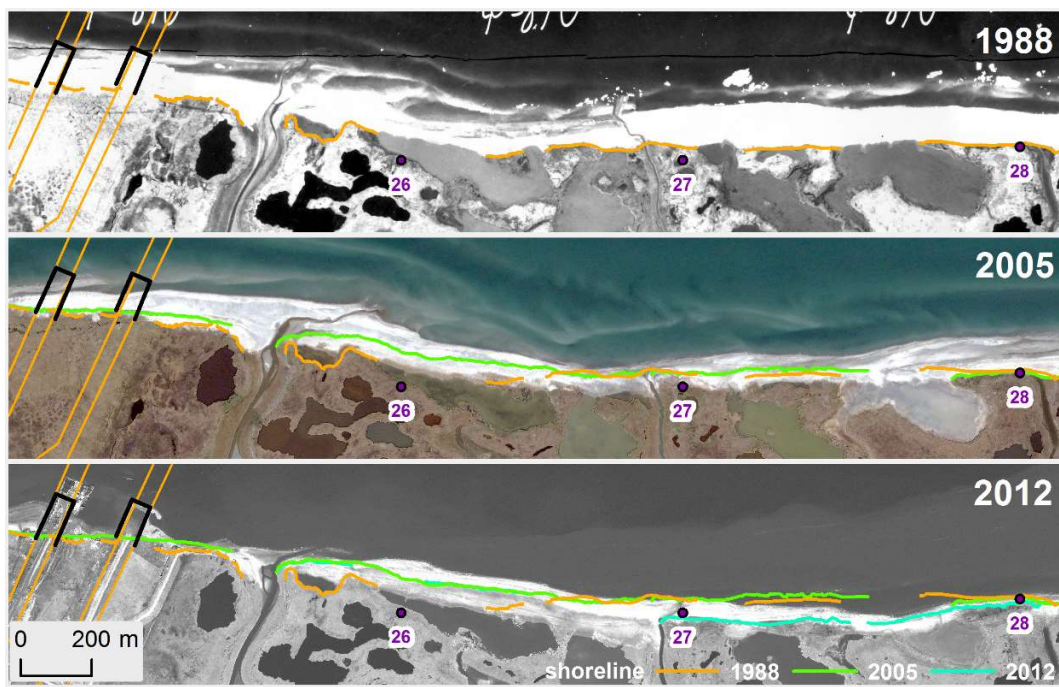


**Figure 8.** Accumulative coast in the east of the Ural key site. Background: 1988—airial image; 2005—QuickBird-2; 2012—WorldView-1.

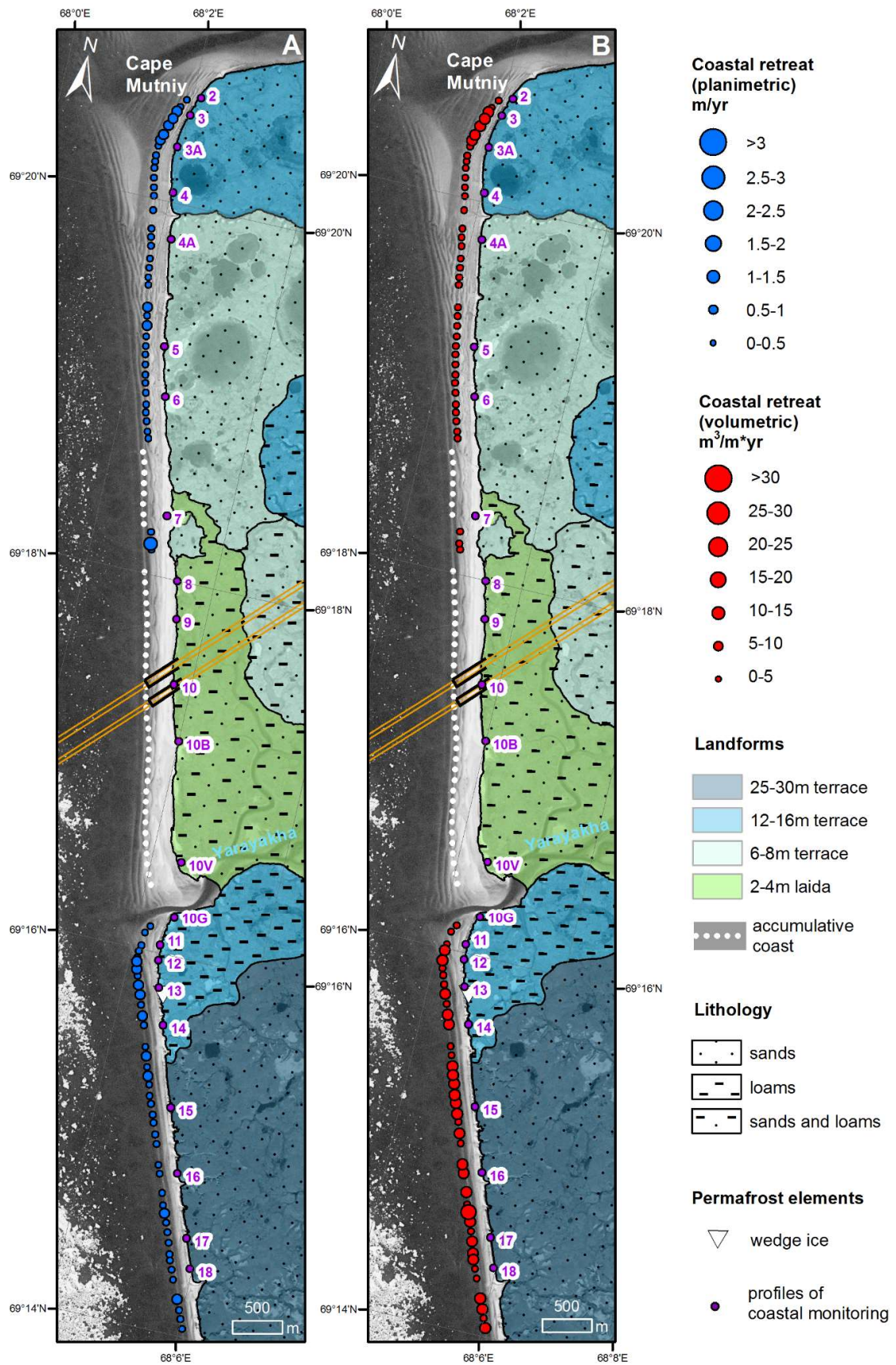


**Figure 9.** Coastal retreat at the Yamal key site: (A) planimetric, and (B) volumetric. Orange lines show gas pipelines; black lines show the cofferdams. Background: Corona KH-4 (1968).

#### 4.2.1. Erosional Coasts

Within the entire coastal segment, both planimetric and volumetric average retreat rates from 1968 to 2016 showed little variability (Figure 9). To the south of the Yarayakha River mouth, the volume of the eroded material was slightly higher than in the northern part of the segment. Different landforms also showed little variability in retreat rates: for high terraces of 25–30 m, medium terraces of 12–16 m, and low terraces of 6–8 m, mean planimetric retreat rates were equal (0.3 m/yr, Table 6). Accordingly, most sediments were eroded from high terraces ( $6.4 \text{ m}^3/\text{m}/\text{yr}$ ), when compared to medium terraces ( $4.8 \text{ m}^3/\text{m}/\text{yr}$ ) and low terraces ( $1.3 \text{ m}^3/\text{m}/\text{yr}$ ).

The most significant coastal retreat was observed in the northern part of the key site near Cape Mutniy (between profiles 3 and 3A, about 1 m/yr) and to the south from the Yarayakha River mouth (profiles 12 and 13, about 0.6 m/yr), where the terrace of 12–16 m was eroded. A large lake (up to 350 m in diameter) was drained as a result of the erosion of the segment between profiles 3A and 4 between 2005 and 2016. The largest volumes of deposits (about  $10 \text{ m}^3/\text{m}/\text{yr}$ ) were eroded from the southern sector of the high (25–30 m) terrace between profiles 16 and 17.

Speaking of temporal variability of coastal retreat (Figure 10), in the last decade, the coastline degraded three times faster than earlier (0.6 m/yr in contrast to 0.2 m/yr from 1988 to 2005) and two times faster than the mean rate for the whole period of 1968–2016. During this period, volumetric retreat ( $6.4 \text{ m}^3/\text{m}/\text{yr}$ ) was two times greater than during the previous periods ( $1.5 \text{ m}^3/\text{m}/\text{yr}$  from 1968 to 1988 and  $3.4 \text{ m}^3/\text{m}/\text{yr}$  from 1988 to 2005) and than the mean value ( $3.7 \text{ m}^3/\text{m}/\text{yr}$ ).

#### 4.2.2. Accumulative Coasts

Before the gas pipeline construction, the coastal segment within the laida (between profiles 7 and 10 V, Figure 11) was relatively stable; based on its topography, it was considered to be accumulative. However, in 2005–2016, substantial changes happened. The dense vegetation boundary retreated by up to 140 m. The greatest retreat was observed on the 1 km long segment to the north of the Yaryakha River mouth, where a port was constructed (profile 10 V, Figure 11). To the north of the recently built cofferdams, the coast retreated by up to 20–50 m. As a result, the vegetation cover was destructed, while the beach moved landward; its width decreased. Consequently, two lakes of up to 60 m in diameter situated between 7 and 8 profiles were drained.

#### 4.3. Hydrometeorological Factors of Coastal Dynamics

According to our estimations, by 2015, total hydrometeorological stress increased by about 100% as compared to the beginning of the 1980s (Figure 12). The air thawing index increased by 40–45% ( $6.65\text{--}7$  degree-days per year for the Yamal and the Ural coasts accordingly); the wave energy grew by about 55–60% compared to the 1979–1984 mean. All of the trends were significant at 0.05 level. The wave energy growth was mainly driven by ice-free period extension, which increased by about 40 days (50%) for Ural coast and by 25 days (35%) for the Yamal coast in 40 years.

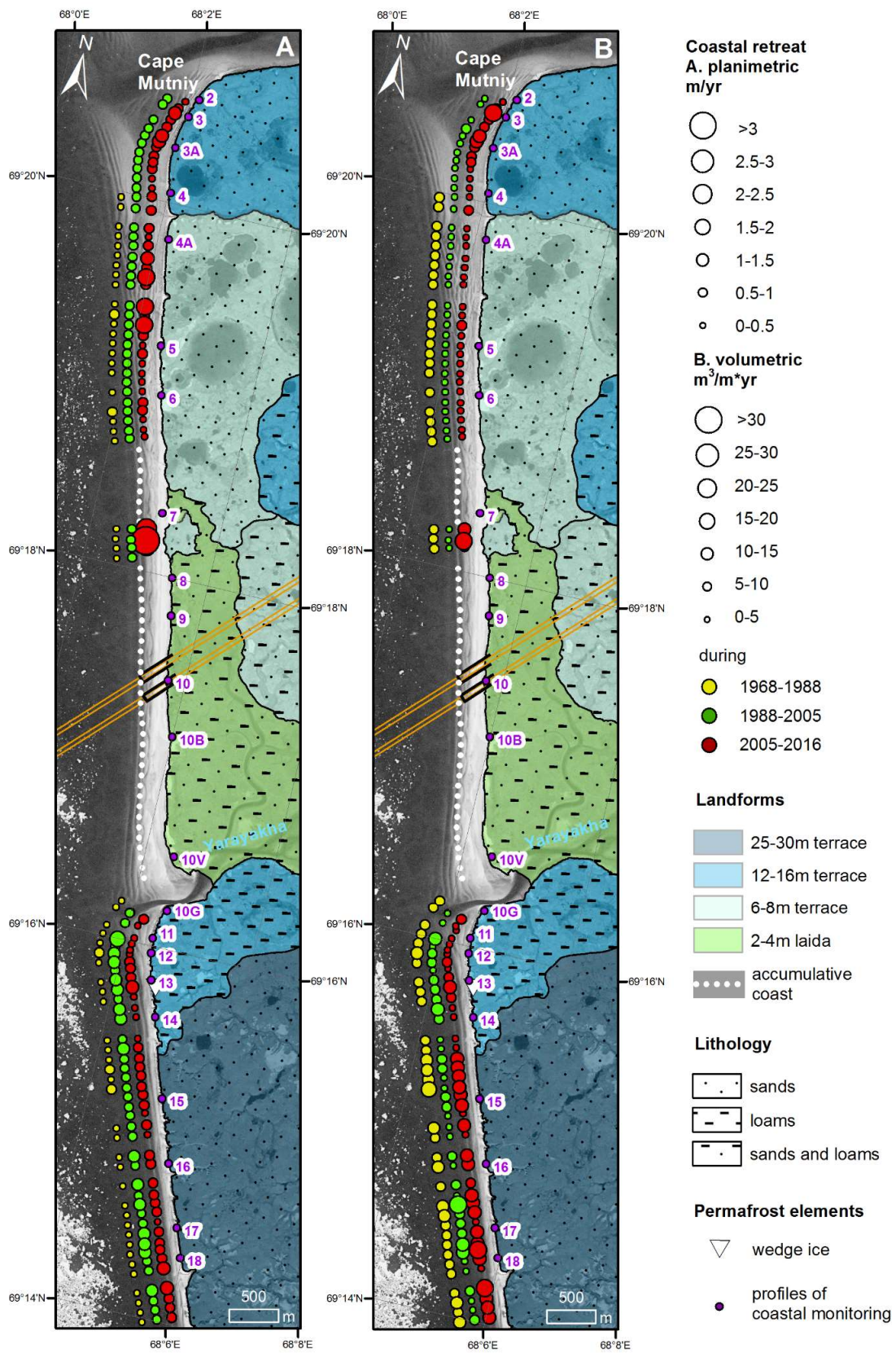


**Figure 10.** Coastal retreat during different periods at the Yamal area: (A) planimetric, and (B) volumetric. Orange lines show gas pipelines; black lines show the cofferdams. Background: Corona KH-4 (1968).

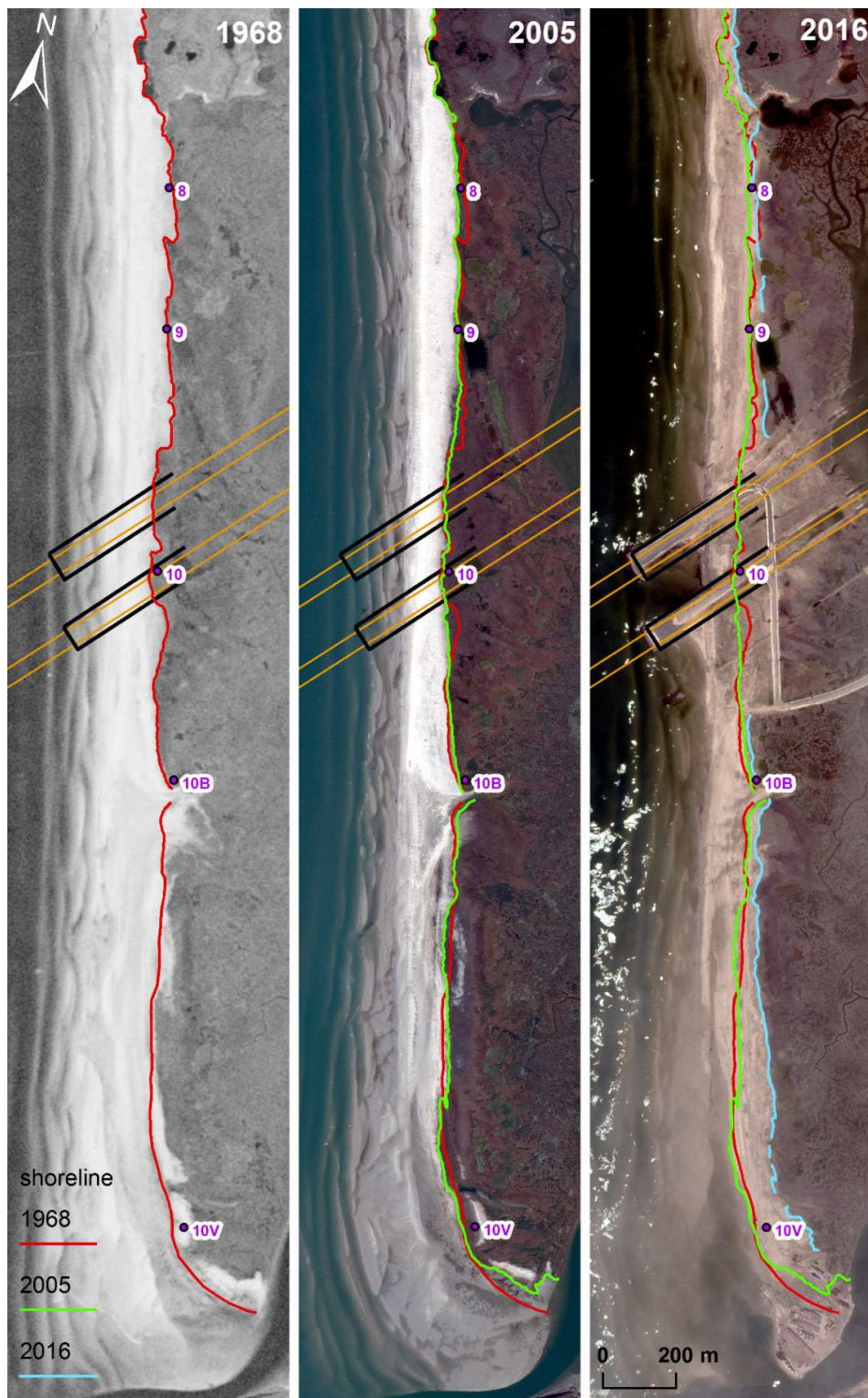


**Figure 11.** Accumulative coast at Yamal key area. Background: 1968—Corona KH-4; 2005—QuickBird-2; 2016—WorldView-3.

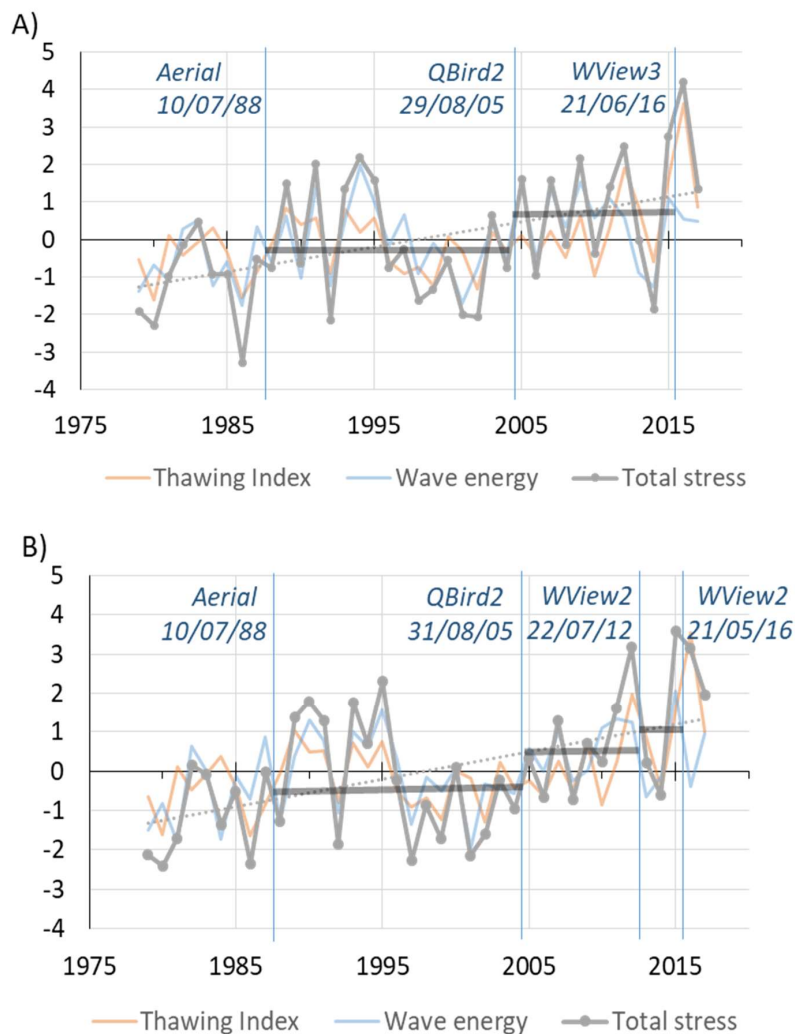


**Figure 12.** Evolution of hydrometeorological factors of coastal dynamics in 1979–2017 for the Yamal (A) and Ural (B) key sites: air thawing index, wave energy flux and total stress (in anomalies divided by standard deviation). Blue vertical lines indicate dates of aerial and satellite imagery (Table 2), solid horizontal—mean values of total stress for the corresponding periods, dashed line—the total stress linear trend.

In 1997–2004, there was a local minimum of both wave-energy (including ice-free period duration) and thermal factors, observed over the entire Barents-Kara region [13]. This minimum was linked to calming of westerly and north-westerly winds, which are wave-dangerous for the region and bringing warmth. The period of 1989–1996 and 2005–2017 were characterized by positive anomalies. The several latest years (2012, 2015, and 2016) revealed an exceptionally high coastal erosion hydrometeorological potential, firstly due to extremely hot summers. At the same time, there were potentially “calm” (relatively cold and not stormy) 2013 and 2014, especially on the Yamal coast.

## 5. Discussion

### 5.1. Application of Remote Sensing for Studies of Coastal Dynamics in the Kara Sea Region

Remote sensing has shown its good applicability for studies of coastal erosion in permafrost areas of Western Siberia. It provides detailed, reliable, and comprehensive information on coastal dynamics. The great advantage of aerial and space imagery application is their easy accessibility due to relatively low price and large coverage. In remote areas with high transportation expenses, such as the Kara Sea

region, remote sensing data may replace, or considerably complement, fieldwork. Moreover, if field monitoring on the coasts of Baydaratskaya Bay was launched in the 1980s, the first satellite imagery for this region was acquired in the 1960s, which allows to extend the period of studies. Another advantage of remote sensing is the possibility to obtain a spatially continuous record of coastal retreat, contrarily to surveys along profiles, where sections with the highest retreat rates may be situated between profiles, and thus, remain unobserved. For instance, at the Yamal coast, the greatest erosion rates fall into the area south of profile 7 (Figure 6A), uncovered by field measurements. Using DEMs allows relatively precise estimation of volumes of eroded material, which is especially important in the application of studies of sediment fluxes, carbon fluxes, etc. [30,62].

However, working with remote sensing data for coastal dynamics studies, we faced some issues. Firstly, the accuracy of the obtained data was relatively low and required improvement: 0.15–0.45 m/yr for planimetric rates while the values of these rates were 0.1–5 m/yr, and 1.1–10 m<sup>3</sup>/m/yr for volumetric rates while the values of these rates were 0.5–20 m<sup>3</sup>/m/yr. The uncertainties could be decreased by obtaining imagery with higher spatial resolution, more thorough georeferencing, and orthorectification of the imagery using stereopairs. Nevertheless, the erosion rates calculated using remote sensing methods showed good agreement with field monitoring data. Coastal retreat rates that were obtained by direct measurements from stable benchmarks for separate profiles had higher accuracy than the rates calculated from aerial and satellite imagery (up to 0.1 m/yr). The average retreat rates for the Ural coast from 1988 to 2016 were estimated as  $1.4 \pm 0.15$  m/yr by aerospace imagery, as compared to  $1.6 \pm 0.1$  m/yr according to observational data. For the Yamal coast, the 1988–2016 average rates obtained by remote sensing data analysis were  $0.4 \pm 0.16$  m/yr, compared to  $0.6 \pm 0.1$  m/yr according to field surveys. Therefore, remote sensing data provided relatively accurate results in assessing long-term erosion rates at large sections.

Additionally, it may be complicated to provide necessary temporal coverage by images due to their low frequency of acquisition or their high cost. It is especially significant while studying the dynamics of accumulative coasts, which are often more changeable and have no direct trend of migration. New remote sensing techniques, such as LiDAR and structure from motion by UAV images, provide more precise and recurrent data [33,35]. Although estimating temporal variability of coastal dynamics using aerospace imagery is limited, they allow drawing general conclusions about changes in retreat rates over time.

## 5.2. Drivers of Coastal Dynamics

Based on aerial and satellite imagery interpretation and field data with regard to the previously published studies, we propose the following main drivers of coastal dynamics in the study region and investigate their spatial and temporal variability. Temporal variability of coastal dynamics was determined chiefly by the weather conditions, which were hard to detect with the help of remote sensing. In this regard, in the paper, we focus mainly on the factors of spatial variability of coastal dynamics.

### 5.2.1. Spatial Variability of Coastal Dynamics

#### Exposure of the Coasts

Exposure of the coast to the waves from the open sea generally determines regional-scale variability of coastal retreat, as coastlines in permafrost areas are usually relatively straight, and their exposure does not vary significantly at a given site. The location of two coasts of Baydaratskaya Bay in relation to other shores and islands is presumably the main factor in determining the difference in their average long-term retreat rates. Coasts of the Ural site are eroded four times faster than coasts at Yamal because of their exposure to the NNE winds and strong waves from the open sea. The Yamal coasts, on the contrary, face to the southwest, with a relatively small wave fetch. They are protected from high waves by the Marresal'skie Koshki Islands. The exposure of the coastal segment, therefore,

influences the whole key area, not separate landforms or profiles. It also plays an especially important role, because the climatic and geologic conditions on both coasts are relatively similar. Local-scale spatial variability within the key sites is governed by other factors.

### Sediment Balance and Longshore Sediment Fluxes

On the Yamal coast, the zone of divergence of longshore wave energy fluxes determines the area with the greatest average multiannual retreat rates to the south of the Yarayakha river mouth near profiles 17 and 18 (Figure 9). The main longshore flux starting from here is directed towards the north, to Cape Mutniy; the second one comes to the south. As a result, this coastal segment experiences high planimetric retreat (0.6 m/yr) and the greatest volumetric erosion ( $10 \text{ m}^3/\text{m}/\text{yr}$ ).

On the Ural coast, the longshore wave energy flux is directed to the south-east along the coast. Due to this, in undisturbed conditions prior to the pipeline construction (in 1964–1988 and in 1988–2005), on the sector of profiles 12–22 (Figure 7), the sediment flux was deficient [46] and coastal erosion prevailed. To the southeast (profiles 26–29), the flux was overloaded and sediments accumulated. After the construction, the westerly (entering) angle of the cofferdams served as a sediment trap; consequently, laidas near profiles 26–29 retreated at catastrophic rates between 2005 and 2012 (Figure 7). The beach to the east of the cofferdams also retreated by 80 m in 2005–2012 (Figure 8).

An example of natural processes that are connected with sediment redistribution in the coastal zone is the segment near profile 11 on the Ural coast, on an isolated remnant of the 6–8-m terrace (Figure 7). In 1964, a spit formed at the mouth of the Ngoyuyakha River. Then, in 1988, the channel dividing the spit from the bluff became inactive, and the spit served as coastal protection. As a result, in 1964–2005, the coast experienced very little retreat. In 2005, the old spit started to erode by longshore wave energy fluxes, and a new spit started to grow at the Ngoyuyakha River mouth. As the spit no longer protected the coast, erosion experienced acceleration, which started in 2005–2012 and continued in 2012–2016. From 2012 to 2016, the retreat rates rose by seven times, as compared to 1964–1988 (about  $20 \text{ m}^3/\text{m}/\text{yr}$  compared to about  $3 \text{ m}^3/\text{m}/\text{yr}$ , accordingly, Figure 7). Such fast erosion was caused by natural cyclic processes of sediment redistribution in spite of a wind-wave energy decrease in 2012–2016, while the rest of the coastline became relatively stable.

Generally, data on the Ural coast showed a shift of the greatest erosion rates from the west to the east (starting at profiles 15–17 in 1964–1988 and moving towards profiles 19–21 in 2012–2016). Such behavior might be caused by changes of the longshore sediment fluxes as a result of a change in the sedimentation regime after the shift of the mouth of the Ngoyuyakha River to the west. A similar situation was described near Kharasavey settlement, Western Yamal [19], where a shift of the zone of divergence of longshore wave energy fluxes determined the shift of maximal retreat rates' spatial distribution.

### Morphology of the Coasts

The height and morphology of the coastal bluffs is essential in speaking of planimetric retreat spatial distribution. A storm that causes slight retreat of high cliff (with large volumes to erode) can provoke sudden and dramatic changes on low coasts. Little material needs to be washed off for their catastrophic linear retreat. Therefore, theoretically low coasts are more vulnerable to erosion rather than high coasts, however in fact it does not work always [1,63]. According to previous estimations [64], laidas of the Ural coasts were considered one of the most stable segments in the area: 0.4–0.6 m/yr retreat from 1988–2006. However, according to our results, from 2005–2012, their erosion accelerated greatly, resulting at almost 10.0 m/yr linear retreat at some locations, with average rates for laidas reaching 7.0 m/yr.

The morphology and width of beaches and tidal flats, which are difficult to assess on satellite imagery because of the varying sea level (the tidal range is 0.8–1.1 m, the surge height is up to 1.5 m [46]), also play an important role in spatial variability of coastal bluffs' retreat [63]. Beaches and tidal flats protect the cliffs from destruction [65]; their width and inclination are one of the main coastal

stability parameters [66]. The greatest deformations of marine accumulative surfaces estimated for the Kara Sea region (Marresale) reached 0.3 m down in 2010 [43]. On the Ural coast of Baydaratskaya Bay, the width of beaches significantly grew in 2005–2016 near the bluffs of the 12–16-m terrace (profiles 15–17, Figure 7). As a result, these coasts were relatively stable from 2012–2016, when compared to the adjacent segments near profiles 19–21.

### Lithology and Ground Ice

The general pattern of erosion rates' distribution showed that they were relatively uniform at the Yamal coasts, with few spatial changes, while at the Ural coasts, the retreat rates varied greatly from segment to segment, and the position of the fastest retreating segments changed through time. We suppose that the main factors causing such difference are sediment composition and ground ice content in the bluffs. All levels of coastal plains at Yamal were predominantly composed by sand; no significant outcrops of large massive ice beds were found [51]. On the contrary, cliffs of the Ural coast had a heterogeneous lithological composition: sands, silts, clays, and peat outcrop at different segments. Large massive ice beds of up to 80 m in length and 4 m in thickness were found at higher bluffs [51], while cliffs that were lowered by thermokarst contained wedge ice networks. This created great spatial variability between small segments. Dallimore et al. [67] showed that the presence of different types of ground ice facilitates coastal erosion. With growth of ground ice content capacity of the coasts for erosion rises, at least on the local settings [68,69]. High ice content creates favorable conditions for extremely fast retreat [37,38], especially under the conditions of climate warming [26]. Increased erosion rates in areas of high ice content in sediments were also noted for the Marresale area, Kara Sea: an ice content increase from 10% to 60% provokes the growth of erosion rates by 1.5–2 times [70,71]. In the eastern part of the Arctic, on the Laptev Sea coasts, the average retreat rates for the Ice Complex segments are 1.9 m/yr, when compared to 0.3 m/yr for areas without the Ice Complex [72].

However, although both sediment composition and ice content influence retreat rates, they are not directly connected. The presence of ground ice, on the one hand, leads to a faster thawing of the bluff. On the other hand, when frozen, the icy cliff can be resistant to waves, similarly to lithified rocks. The amount of heat required for thawing of the ice increases as well, slowing down the erosion. However, excessive ice content leads to a deficiency of sediment flux to the coastal zone and consecutive erosion enhancement [3,66]. The influence of sediment composition on coastal retreat rates can be two-fold, as well. Loams at the base of a 6–8-m terrace on the Ural coast occasionally form a step and they retreat more slowly than the overlying sands. On the other hand, with their erosion, less beach-forming material arrives on the beach, the deficit of which contributes to the accelerated erosion of the coastal bluffs.

In this way, no direct correlation between sediment composition and ground ice presence can be done at every exact small segment; at the same time, the degree of erosion rates' spatial variability at the level of the whole key area clearly depends on these factors.

### 5.2.2. Temporal Variability of Coastal Dynamics

The temporal variability of erosion rates is linked to changes of hydrometeorological conditions: the thermal and wind-wave energy factors combining and enhancing each other. With ongoing climate warming, both air temperature and wind-wave energy increase and enhance the risks of catastrophic coastal erosion processes; however, their changes are not simultaneous and they do not always directly relate to coastal erosion rates [25].

Our results showed a general increase of coastal erosion rates from the 1960s to 2012. This agrees well with estimations of the total hydrometeorological stress on our sites (Figure 12) and for the Barents-Kara region in general [73]. The peak erosion rate values typical for 2005–2012 coincided with high hydrometeorological stress [73]. Still, the subsistent high total stress in 2013–2015 did not result in high retreat rates in this period. The reason is that total stress was low during two previous years.

For the 12–16 m terrace this led to a temporary stop in erosion. The energy of the storms of 2015 was spent on the removal of material that had come to the beach in previous years. The thermal factor could also begin to work only after the removal of the thawed sediment by waves. Therefore, despite the high total stress in 2015, the retreat rates for this period in comparison with the rates of 1988–2005 were the same for high terraces and for the 2–4 m laida. That is to say, the higher the shore is, the less resistant it is to changes in hydrometeorological forcing. The rates of retreat of higher shores in a particular year are determined not only by the situation of this year, but also by the combination of wave energy and the thermal factor in previous years.

Before the recent climate change, the Arctic coasts experienced a long, 9–10-month period of conservation when the bluffs and sea were covered by ice and snow [26,66]. As a result of sea ice extent decline, autumn storms fell into the ice-free period causing significant retreat. This was especially noticeable in 2005, when the wind-wave energy was even higher than later in 2012 on both Yamal and Ural coasts [58]. Such increases in wind-wave energy affect all coasts. From the example of the Alaskan coasts, it was found that storm frequency shows the best correlation with erosion rates, contrarily to temperature and precipitation [73]. On the Ural coast, storm surges of 2009–2010 [43] provided catastrophic retreat of the laida coasts.

The wind-wave energy is the main factor determining the retreat of the Yamal coast; however, for the Ural coast, both the thermal and wind-wave energy factors are important [74]. Therefore, the Ural coast turns out to be more vulnerable to the ongoing climatic changes. The summers from 2005 to 2012 were relatively warm, causing active thawing of the coastal bluffs. Positive air temperatures prevailed for about five months [75].

Generally, within most of the Arctic coasts, a growth of erosion rates was observed since the beginning of the 2000s [26,30,75]. However, periods of active retreat alternate with years of low erosion. Such is the case of Baydaratskaya Bay in 2012–2016, when coastal erosion was even smaller than in the 20th century. The main reason for that was the relatively low wind-wave energy (despite high temperatures). This shows that in spite of the general increase of erosion rates with climate change, this rising trend is imposed by cyclic fluctuations, proved for both the Russian [21,25,43] and Canadian [67] Arctic.

### 5.2.3. Human Impact on Coastal Dynamics

As the underwater pipeline crossing of Baydaratskaya Bay was constructed in 2008–2012, human activity could have an impact on the erosion rates of 2005–2012 and 2012–2016 only. Indeed, in 2005–2012 and in 2005–2016, erosion rates increased by up to several times on the Ural and Yamal coast, accordingly. However, this increase coincided with high values of wind-wave energy in 2005–2012 (Figure 12 and [26]), that make it challenging to distinguish natural and human-induced processes.

At the same time, clear evidence of the construction's impact on the spatial distribution of erosion rates can be noted. The most prominent example is the redistribution of the sediment fluxes by cofferdams. In their angles directed towards the longshore sediment flux direction, accumulation starts; as a result, areas that are behind the cofferdams get eroded. On the Ural coasts, this happened to profiles 26–28, originally accumulative and stable, where coastal retreat of 2–8 m/yr happened between 2005 and 2012. The maximum rates of retreat of low laida were caused by the disturbance of the vegetation cover by heavy vehicles. The rest of the coastline did not experience so much technogenic pressure, as the longshore sediment flux is directed to the southeast. Therefore, the erosional coasts were not influenced by the cofferdams' construction.

On the Yamal coast, the sediment flux near the cofferdams is directed northwards. As a result of enhanced erosion behind the cofferdams, the 6–8 m terrace near profile 7 (Figure 7) experienced record high retreat rates of more than 3 m/yr from 2005 to 2016, while in the rest of the territory, such an increase was smaller (not more than 2.5 m/yr). Accumulative segments near profiles 8–9, which were previously considered stable, also retreated considerably in 2005–2016 (Figure 11).

Another example of disturbed sediment balance is dredging around the port at the Yarayakha River mouth at Yamal, seen in satellite images of 2016, which will presumably cause retreat of areas near profiles 10–10V in the years to come. Movement of transport along the beach and on terraces also changes the sediment balance and provokes thermoerosion and thermokarst. In 2005, to the east of the cofferdams, there was evidence of thermokarst along an old road, clearly seen in the satellite image. Disturbance and degradation of vegetation can also cause the disturbance of the thermal regime of solis and the degradation of permafrost and trigger thermoerosion, soil subsidence, and aeolian processes.

## 6. Conclusions

Remote sensing is a powerful tool in coastal dynamics studies. It is especially relevant in terms of the remoteness and difficult accessibility of Arctic coasts. Despite some of the issues that we faced while working with remotely sensed data, such as relatively low accuracy and a lack of time lapses, we obtained reliable and valid data on coastal dynamics. Based on multi-temporal high resolution aerial and space images and DEMs, we calculated planimetric and volumetric rates of retreat as an integrative estimation of coastal erosion. Remote sensing and field data on geomorphological, lithological, and permafrost conditions allowed us to estimate their contribution to the coastal dynamics.

For the Ural coast, higher erosion rates were typical compared to the Yamal coast. Average rates of retreat of erosional segments of the Ural coast were  $1.2 \pm 0.15$  m/yr and  $8.7 \pm 1.4$  m<sup>3</sup>/m/yr from 1964 to 2016; erosional segments of the Yamal coast were eroded with rates of  $0.3 \pm 0.16$  m/yr and  $3.7 \pm 2.1$  m<sup>3</sup>/m/yr from 1968 to 2016. Thus, the retreat of the Ural coast was faster and the retreat of the Yamal coast was slower than the average linear erosion rate for the entire Arctic (0.5 m/yr) [76]. Despite the fact that the key areas were located at the coast of a shallow gulf, the rates of retreat were comparable to those at Western Yamal key sites, at the open coast of the Kara Sea (1.1 m/yr for Kharasavey area [19] and 1.7 m/yr for Marresale area [43]). Higher erosion rates at the Ural coast were determined, above all, by its exposure to northerly and north-easterly waves from the open sea. Coastal retreat rates showed significant variability at the Ural key site, while at Yamal, their spatial distribution was uniform. Such local-scale spatial variability is caused by heterogeneous lithology of the Ural key site and the presence of massive ice beds, contrarily to Yamal, where all the bluffs are composed of sand with relatively low ice content.

Remote sensing and field data on geomorphological, lithological, and permafrost conditions allowed us to estimate their contribution to the coastal dynamics. The most intense erosion (up to 9 m/yr) occurred at low laidas with high ice content at the Ural coast in 2005–2012. Lower coastal bluffs tended to be less stable under changing hydrometeorological forcing.

The analysis of temporal variability of coastal retreat rates showed a tendency of their increase since the 1960s associated with climate warming in the Arctic. The temporal variability of the retreat rates is well explained by variability of the thawing index and wave energy flux. We relate sharp acceleration of erosion in 2005–2012 with the increase of wind-wave and thermal impact superimposed on human activity.

**Author Contributions:** A.N. Lithology and Geomorphology Field Data Collection and Interpretation, Processing Remote Sensing Data and its Interpretation, Map Creation, Paper Writing and Preparation; N.B. Permafrost Field Data Collection and Interpretation, Processing Aerial and Space Imagery and its Interpretation, Topographic Survey and its Interpretation, Paper Writing (Results), Review and Editing; A.B. Field and Remote Sensing Data Interpretation, Conceptualization, Paper Writing (Discussion), Review and Editing; D.A. Lithology and Permafrost Field Data Collection and Interpretation, Topographic Survey and its Interpretation, Paper Writing (Study Area); A.M. Background and Regional Settings, Resources, Paper Writing (Introduction); E.Z. Uncertainty Assessment, Software, Paper Writing (Methodology); N.S. Climatic Settings, Paper Writing (Discussion); S.O. Lithology and Geomorphology Field Data Collection and Analysis, Project Administration, Conceptualization, Supervision, Funding Acquisition, Review and Editing.

**Funding:** Remote sensing data analysis was accomplished with the financial support of the Russian Science Foundation project No.16-17-00034. Analysis of human impact on coastal systems was executed with the support of the Russian Science Foundation project No.17-77-10130. Hydrometeorological factors of coastal dynamics were assessed with the support of the Russian Science Foundation project No.14-37-00038. Permafrost data

collection and interpretation were conducted with financial support of Russian Foundation for Basic Research project No.16-35-60099 mol\_a\_dk.

**Acknowledgments:** We thank Digital Globe Foundation© for providing us with imagery of WorldView-2 (2016) for the Ural study area, and QuickBird-2 (2005) and WorldView-3 (2016) for the Yamal study area. We also thank the SAMCoT project for the WorldView-1 (2012) and WorldView-2 (2013) for the Ural study area. We are very grateful to Pavel Ivanov, Friderich Shiller University Jena, for manuscript revision and English editing.

**Conflicts of Interest:** The authors declare no conflict of interest.

## References

1. Lantuit, H.; Overduin, P.P.; Wetterich, S. Recent progress regarding permafrost coasts. *Permafr. Periglac. Process.* **2013**, *24*, 120–130. [CrossRef]
2. Kizyakov, A.I.; Leibman, M.O.; Perednya, D.D. Destructive relief-forming processes at the coasts of the Arctic plains with tabular ground ice. *Earth's Cryosphere* **2006**, *2*, 79–89. (In Russian)
3. Are, F.E. *Coastal Erosion of the Arctic Lowlands*; Academic Publishing House “Geo”: Novosibirsk, Russia, 2012; p. 291. ISBN 978-5-904682-70-5. (In Russian)
4. Bates, N.R.; Mathis, J.T. The Arctic Ocean marine carbon cycle: Evaluation of air-sea CO<sub>2</sub> exchanges, ocean acidification impacts and potential feedbacks. *Biogeosciences* **2009**, *6*, 2433–2459. [CrossRef]
5. Semiletov, I.P.; Pipko, I.I.; Shakhova, N.E.; Dudarev, O.V.; Pugach, S.P.; Charkin, A.N.; McRoy, C.P.; Kosmach, D.; Gustafsson, Ö. Carbon transport by the Lena River from its headwaters to the Arctic Ocean, with emphasis on fluvial input of terrestrial particulate organic carbon vs. carbon transport by coastal erosion. *Biogeosciences* **2011**, *8*, 2407–2426. [CrossRef]
6. Vonk, J.E.; Sánchez-García, L.; Van Dongen, B.E.; Alling, V.; Kosmach, D.; Charkin, A.; Semiletov, I.P.; Dudarev, O.V.; Shakhova, N.; Roos, P.; et al. Activation of old carbon by erosion of coastal and subsea permafrost in Arctic Siberia. *Nature* **2012**, *489*, 137–140. [CrossRef] [PubMed]
7. Climate Change 2013: The Physical Science Basis. *Contribution of Working Group I to the Fifth Assessment Report of the Intergovernmental Panel on Climate Change*; Stocker, T.F., Qin, D., Plattner, G.K., Eds.; Cambridge University Press: Cambridge, UK; New York, NY, USA, 2013; p. 1535. ISBN 978-1-107-66182-0. Available online: [http://www.climatechange2013.org/images/report/WG1AR5\\_ALL\\_FINAL.pdf](http://www.climatechange2013.org/images/report/WG1AR5_ALL_FINAL.pdf) (accessed on 15 April 2018).
8. Climate Change 2014: Synthesis Report. *Contribution of Working Groups I, II and III to the Fifth Assessment Report of the Intergovernmental Panel on Climate Change*; Core Writing Team; Meyer, L.A., Ed.; IPCC: Geneva, Switzerland, 2014; p. 151. ISBN 978-92-9169-143-2. Available online: <http://www.ipcc.ch/report/ar5/syr/> (accessed on 15 April 2018).
9. Parkinson, C.L.; DiGirolamo, N.E. New visualizations highlight new information on the contrasting Arctic and Antarctic sea-ice trends since the late 1970s. *Remote Sens. Environ.* **2016**, *183*, 198–204. [CrossRef]
10. Barber, D.G.; Meier, W.N.; Gerland, S.; Mundy, C.J.; Holland, M.; Kern, S.; Li, Z.; Michel, C.; Perovich, D.K.; Tamura, T.; et al. Arctic sea ice. In *Snow, Water, Ice and Permafrost in the Arctic (SWIPA) 2017*; Arctic Monitoring and Assessment Programme (AMAP): Oslo, Norway, 2017; pp. 103–136. ISBN 978-82-7971-101-8. Available online: <https://www.amap.no/documents/download/2987> (accessed on 5 April 2018).
11. Atkinson, D.E. Observed storminess patterns and trends in the circum-Arctic coastal regime. *Geo-Mar. Lett.* **2005**, *25*, 98–109. [CrossRef]
12. Savo, V.; Lepofsky, D.; Benner, J.P.; Kohfeld, K.E.; Bailey, J.; Lertzman, K. Observations of climate change among subsistence-oriented communities around the world. *Nat. Clim. Chang.* **2016**, *6*, 462–473. [CrossRef]
13. Shabanova, N.; Ogorodov, S.; Shabanov, P.; Baranskaya, A. Hydrometeorological forcing of western russian arctic coastal dynamics: Xx-century history and current state. *Geogr. Environ. Sustain.* **2018**, *11*, 113–129. [CrossRef]
14. Meyssignac, B.; Cazenave, A. Sea level: A review of present-day and recent-past changes and variability. *J. Geodyn.* **2012**, *58*, 96–109. [CrossRef]
15. Lantuit, H.; Pollard, W.H. Fifty years of coastal erosion and retrogressive thaw slump activity on Herschel Island, southern Beaufort Sea, Yukon Territory, Canada. *Geomorphology* **2008**, *95*, 84–102. [CrossRef]

16. Kritsuk, L.N.; Dubrovin, V.A.; Yastreba, N.V. Some results of integrated study of the Kara Sea coastal dynamics in the Marre-Sale meteorological station area, with the use of GIS technologies. *Earth's Cryosphere* **2014**, *4*, 59–69.
17. Pizhankova, E.I. Modern climate change at high latitudes and their influence on the coastal dynamics of the Dmitriy Laptev Strait area. *Earth's Cryosphere* **2016**, *1*, 51–64.
18. Maslakov, A.; Kraev, G. Erodibility of permafrost exposures in the coasts of Eastern Chukotka. *Polar Sci.* **2016**, *10*, 374–381. [[CrossRef](#)]
19. Belova, N.G.; Shabanova, N.N.; Ogorodov, S.A.; Kamalov, A.M.; Kuznetsov, D.E.; Baranskaya, A.V.; Novikova, A.V. Erosion of permafrost coasts of Kara Sea near Kharasavey Cape, Western Yamal. *Earth's Cryosphere* **2017**, *21*, 73–83. [[CrossRef](#)]
20. *The Arctic Coastal Erosion Problem*; (No. SAND2016-9762); Frederick, J.M.; Thomas, M.A.; Bull, D.L.; Jones, C.A.; Roberts, J.D. (Eds.) Sandia National Lab.(SNL-NM): Albuquerque, NM, USA; Sandia National Laboratories: Carlsbad, NM, USA, 2016; p. 122. ISBN 978-92-9169-143-2.
21. Vasiliev, A.; Kanevskiy, M.; Cherkashov, G.; Vanshtein, B. Coastal dynamics at the Barents and Kara Sea key sites. *Geo-Mar. Lett.* **2005**, *25*, 110–120. [[CrossRef](#)]
22. Obu, J.; Lantuit, H.; Fritz, M.; Pollard, W.H.; Sachs, T.; Günther, F. Relation between planimetric and volumetric measurements of permafrost coast erosion: A case study from Herschel Island, western Canadian Arctic. *Polar Res.* **2016**, *35*, 30313. [[CrossRef](#)]
23. Pizhankova, E.I. Termodenudation in the coastal zone of the Lyakhovsky islands (interpretation of aerospace images). *Earth's Cryosphere* **2011**, *3*, 61–70. (In Russian)
24. Grigoriev, M.N.; Razumov, S.O.; Kunitzkiy, V.V.; Spektor, V.B. Dynamics of the Russian East Arctic Sea coasts: Major factors, regularities and tendencies. *Earth's Cryosphere* **2006**, *4*, 74–95. (In Russian)
25. Vasiliev, A.A.; Streletskaaya, I.D.; Cherkashev, G.A.; Vanshtein, B.G. Coastal dynamics of the Kara Sea. *Earth's Cryosphere* **2006**, *2*, 56–67. (In Russian)
26. Jones, B.M.; Arp, C.D.; Jorgenson, M.T.; Hinkel, K.M.; Schmutz, J.A.; Flint, P.L. Increase in the rate and uniformity of coastline erosion in Arctic Alaska. *Geophys. Res. Lett.* **2009**, *36*. [[CrossRef](#)]
27. Radosavljevic, B.; Lantuit, H.; Pollard, W.; Overduin, P.; Couture, N.; Sachs, T.; Helm, V.; Frit, M. Erratum to: Erosion and Flooding-Threats to Coastal Infrastructure in the Arctic: A Case Study from Herschel Island, Yukon Territory, Canada. *Estuar. Coasts* **2016**, *39*, 1294–1295. [[CrossRef](#)]
28. Farquharson, L.M.; Mann, D.H.; Swanson, D.K.; Jones, B.M.; Buzard, R.M.; Jordan, J.W. Temporal and spatial variability in coastline response to declining sea-ice in northwest Alaska. *Mar. Geol.* **2018**, *404*, 71–83. [[CrossRef](#)]
29. Mars, J.C.; Houseknecht, D.W. Quantitative remote sensing study indicates doubling of coastal erosion rate in past 50 yr along a segment of the Arctic coast of Alaska. *Geology* **2007**, *35*, 583–586. [[CrossRef](#)]
30. Günther, F.; Overduin, P.P.; Sandakov, A.V.; Grosse, G.; Grigoriev, M.N. Short- and long-term thermo-erosion of ice-rich permafrost coasts in the Laptev Sea region. *Biogeosciences* **2013**, *10*, 4297–4318. [[CrossRef](#)]
31. Grosse, G.; Schirrmeister, L.; Kunitsky, V.V.; Hubberten, H.W. The use of CORONA images in remote sensing of periglacial geomorphology: An illustration from the NE Siberian coast. *Permafr. Periglac. Process.* **2005**, *16*, 163–172. [[CrossRef](#)]
32. Jones, B.M.; Stoker, J.M.; Gibbs, A.E.; Grosse, G.; Romanovsky, V.E.; Douglas, T.A.; Kinsman, N.E.M.; Richmond, B.M. Quantifying landscape change in an arctic coastal lowland using repeat airborne LiDAR. *Environ. Res. Lett.* **2013**, *8*, 045025. [[CrossRef](#)]
33. Gonçalves, J.A.; Henriques, R. UAV photogrammetry for topographic monitoring of coastal areas. *ISPRS J. Photogramm. Remote Sens.* **2015**, *104*, 101–111. [[CrossRef](#)]
34. Klemas, V.V. Coastal and environmental remote sensing from unmanned aerial vehicles: An overview. *J. Coast. Res.* **2015**, *31*, 1260–1267. [[CrossRef](#)]
35. Obu, J.; Lantuit, H.; Grosse, G.; Günther, F.; Sachs, T.; Helm, V.; Fritz, M. Coastal erosion and mass wasting along the Canadian Beaufort Sea based on annual airborne LiDAR elevation data. *Geomorphology* **2017**, *293*, 331–346. [[CrossRef](#)]
36. Burn, C.R.; Lewkowicz, A.G. Canadian landform examples-17 retrogressive thaw slumps. *Can. Geogr.* **1990**, *34*, 273–276. [[CrossRef](#)]
37. Are, F.E. Thermal abrasion of sea coasts. *Polar Geogr. Geol.* **1988**, *1*, 1–86. [[CrossRef](#)]
38. Are, F.E. Thermal abrasion of sea coasts. *Polar Geogr. Geol.* **1988**, *2*, 87–157. [[CrossRef](#)]

39. Kizyakov, A.I. The dynamics of thermodenudation processes at the Yugorsky Peninsula coast. *Earth's Cryosphere* **2005**, *9*, 63–67. (In Russian)
40. Leont'yev, I.O. Modeling erosion of sedimentary coasts in the western Russian Arctic. *Coast. Eng.* **2003**, *47*, 413–429. [[CrossRef](#)]
41. Ogorodov, S.; Arkhipov, V.; Kokin, O.; Marchenko, A.; Overduin, P.; Forbes, D. Ice effect on coast and seabed in Baydaratskaya Bay, Kara Sea. *Geogr. Environ. Sustain.* **2013**, *6*, 21–37. [[CrossRef](#)]
42. Ogorodov, S.A.; Baranskaya, A.V.; Belova, N.G.; Kamalov, A.M.; Kuznetsov, D.E.; Overduin, P.; Shabanova, N.N.; Vergun, A.P. Coastal Dynamics of the Pechora and Kara Seas Under Changing Climatic Conditions and Human Disturbances. *Geogr. Environ. Sustain.* **2016**, *3*, 53–73. [[CrossRef](#)]
43. Vasiliev, A.A.; Shirokov, R.S.; Oblogov, G.E.; Streletskaya, I.D. Coastal dynamics of the Western Yamal. *Earth's Cryosphere* **2011**, *15*, 63–65.
44. Yuriev, I.V. Problems of gas field exploitation in the coastal zone of Western Yamal. *Earth's Cryosphere* **2009**, *13*, 46–54. (In Russian)
45. Bulygina, O.N.; Razuvaeva, V.N.; Trofimenko, L.T.; Shvets, N.V. *Description of the Database Massive of Average Monthly Air Temperature at the Stations of Russia*. 2017. Available online: [meteo.ru/data](http://meteo.ru/data) (accessed on 20 May 2018).
46. Baydaratskaya Bay Environmental Conditions. *The Basic Results of Studies for the Pipeline "Yamal-Center" Underwater Crossing Design*; Publishing House "GEOS": Moscow, Russia, 1997; p. 432. ISBN 5-89118-008-1. (In Russian)
47. Romanenko, F.A.; Belova, N.G.; Nikolaev, V.I.; Olyunina, O.S. Sediments of the Yugorsky coast of Baydaratskaya Bay, Kara Sea. Fundamental Problems of Quaternary: Results and Trends of Further Researches. In Proceedings of the Fifth All-Russian Quaternary Conference, Moscow, Russia, 7–9 November 2007; Publishing House "GEOS": Moscow, Russia, 2007; pp. 348–351, ISBN 978-5-89118-401-5. (In Russian)
48. Belova, N.G.; Solomatin, V.I.; Romanenko, F.A. Massive ground ice on the Ural coast of Baydaratskaya Bay, Kara Sea, Russia. In Proceedings of the 9th International Conference on Permafrost, University of Alaska, Fairbanks, AK, USA, 29 June–3 July 2008; pp. 107–112.
49. Romanenko, F.A. Geomorphological types of low coasts of Yamal and Tazovskiy peninsula and their role in forming of shore deposition. In *Geology of Marine and Oceans, Proceedings of the XIX International Conference on Marine Geology, Publishing House "GEOS", Moscow, Russia, 14–18 November 2011*; University of Washington: Washington, DC, USA; Volume 1, pp. 75–79. (In Russian)
50. Forman, S.L.; Ingolfsson, O.; Gataullin, V.; Manley, W.F.; Lokrantz, H. Late Quaternary stratigraphy, glacial limits, and paleoenvironments of the Marresale Area, Western Yamal Peninsula, Russia. *Quat. Res.* **2002**, *57*, 355–370. [[CrossRef](#)]
51. Belova, N.G. *Massive Ice of the Southwestern Coast of the Kara Sea*; MAKS Press: Moscow, Russia, 2014; p. 180. ISBN 978-5-317-04875-4. (In Russian)
52. Romanenko, F.A.; Garankina, E.V.; Shilova, O.S. The stratigraphy of recent sediments at western Yamal Peninsula and topography formation in Late Pleistocene and Holocene. In *Fundamental Problems of Quaternary: Results and Trends of Further Researches, Proceedings of the 6th All-Russian Quaternary Conference, Novosibirsk, Russia, 19–23 October 2009*; Publishing House of Siberian Branch of the Russian Academy of Sciences: Novosibirsk, Russia, 2009; pp. 505–508. (In Russian)
53. United State Geological Survey. Available online: [earthexplorer.usgs.gov](http://earthexplorer.usgs.gov) (accessed on 15 February 2018).
54. Galiatsatos, N.; Donoghue, D.N.; Philip, G. High resolution elevation data derived from stereoscopic CORONA imagery with minimal ground control: An approach using Ikonos and SRTM data. *Photogramm. Eng. Remote Sens.* **2007**, *9*, 1093–1106. [[CrossRef](#)]
55. ArcticDEM. Available online: <https://www.pgc.umn.edu/data/arcticdem/> (accessed on 15 February 2018).
56. Dai, C.; Howat, I.M. Measuring lava flows with ArcticDEM: Application to the 2012–2013 eruption of Tolbachik, Kamchatka. *Geophys. Res. Lett.* **2017**, *44*, 12,133–12,140. [[CrossRef](#)]
57. Thieler, E.R.; Himmelstoss, E.A.; Zichichi, J.L.; Ergul, A. *Digital Shoreline Analysis System (DSAS) version 4.0. An ArcGIS Extension for Calculating Shoreline Change*. U.S. Geological Survey Open-File Report 2008-1278. 2009. Available online: <https://pubs.er.usgs.gov/publication/ofr20081278> (accessed on 5 March 2018).
58. Günther, F.; Overduin, P.P.; Yakshina, I.A.; Opel, T.; Baranskaya, A.V.; Grigoriev, M.N. Observing Muostakh disappear: Permafrost thaw subsidence and erosion of a ground-ice-rich island in response to arctic summer warming and sea ice reduction. *Cryosphere* **2015**, *1*, 151–178. [[CrossRef](#)]

59. Dee, D.P.; Uppala, S.M.; Simmons, A.J.; Berrisford, P.; Poli, P.; Kobayashi, S.; Andrae, U.; Balmaseda, M.A.; Balsamo, G.; Bauer, P.; et al. The ERA- Interim reanalysis: Configuration and performance of the data assimilation system. *Q.J.R. Meteorol. Soc.* **2011**, *137*, 553–597. [CrossRef]
60. EUMETSAT Ocean and Sea Ice Satellite Application Facility. Global sea ice concentration reprocessing dataset 1978–2015 (v1.2, 2015). Available online: <http://osisaf.met.no> (accessed on 14 September 2018).
61. Amante, C.; Eakins, B.W. ETOPO1 1 Arc-Minute Global Relief Model: Procedures, Data Sources and Analysis. In *NOAA Technical Memorandum NESDIS NGDC-24*; National Geophysical Data Center, NOAA: Boulder, CO, USA, 2009.
62. Streletskaia, I.D.; Vasiliev, A.A.; Vanstein, B.G. Erosion of sediment and organic carbon from the Kara Sea coast. *Arct. Antarct. Alp. Res.* **2009**, *1*, 79–87. [CrossRef]
63. Konopczak, A.M.; Manson, G.K.; Couture, N.J. *Variability of Coastal Change along the Western Yukon Coast*; Geological Survey of Canada Open File Report; Geological Survey of Canada: Ottawa, ON, Canada, 2014; 81p.
64. Kamalov, A.M.; Ogorodov, S.A.; Birukov, V.Y.; Sovershaeva, G.D.; Tsvetsinsky, A.S.; Arkhipov, V.V.; Belova, N.G.; Noskov, A.I.; Solomatin, V.I. Coastal and seabed morpholithodynamics of Baydaratskaya Bay at the route of gas pipeline crossing. *Earth's Cryosphere* **2006**, *3*, 3–14. (In Russian)
65. Zenkovich, V.P. *Fundamentals of the Theory about the Development of the Sea Coast*; Publisher Academia of Science of the USSR: Moscow, Russia, 1962; p. 710. (In Russian)
66. *Geoecology of the North: Introduction into Geocryecology*; Solomatin, V.I.; Ushakov, G.B.; Golubchikov, V.A.; Zaytsev, V.I. (Eds.) Moscow State University Publisher: Moscow, Russia, 1992; p. 270. ISBN 978-521-102-370-3. (In Russian)
67. Dallimore, S.R.; Wolfe, S.; Solomon, S.M. Influence of ground ice and permafrost on coastal evolution, Richards Island, Beaufort Sea Coast, NWT. *Can. J. Earth Sci.* **1996**, *33*, 664–675. [CrossRef]
68. Barnhart, K.R.; Overeem, I.; Anderson, R.S. The effect of changing sea ice on the physical vulnerability of Arctic coasts. *Cryosphere* **2014**, *8*, 1777–1799. [CrossRef]
69. Irrgang, A.M.; Lantuit, H.; Manson, G.K.; Günther, F.; Grosse, G.; Overduin, P.P. Variability in rates of coastal change along the Yukon coast, 1951 to 2015. *J. Geophys. Res. Earth Surf.* **2018**, *123*, 779–800. [CrossRef]
70. Vasiliev, A.A. Permafrost controls of coastal dynamics at the Marre-Sale key site, western Yamal. In Proceedings of the 8th International Conference on Permafrost, Zürich, Switzerland, 21–25 July 2003; pp. 1173–1178.
71. Vasiliev, A.A. Some problems of coastal mapping in the Russian Arctic. In *Ber. Polarforsch. Meeresforsch.* 2002, 413. *Arctic Coastal Dynamics*; Report of an International Workshop; Potsdam, Germany, 26–30 November 2001; Brown, J., Solomon, S., Eds.; Alfred Wegener Institute for Polar and Marine Research: Potsdam, Germany, 2002; p. 77.
72. Grigoriev, M.N. Cryomorphogenesis and Lithodynamics of the Coastal-Shelf Zone of the Seas of Eastern Siberia. Ph.D. Thesis, Melnikov Permafrost Institute, Yakutsk, Russia, 2008. (In Russian)
73. Shabanova, N.N.; Ogorodov, S.A.; Romanenko, F.A. Russian arctic coastal dynamics hydrometeorological forcing: Half-century his-tory and current state. In Proceedings of the Coastal Dynamics 2017, Helsingør, Denmark, 12–16 June 2017; pp. 108–116. Available online: [http://coastaldynamics2017.dk/onewebmedia/196\\_shabanova.pdf](http://coastaldynamics2017.dk/onewebmedia/196_shabanova.pdf) (accessed on 15 May 2018).
74. Kopa-Ovdienko, N.V.; Ogorodov, S.A. Peculiarities of dynamics of thermoabrasion coasts of Baydaratskaya Bay (Kara Sea) today. *Geomorphol. RAS* **2016**, *3*, 12–21. (In Russian) [CrossRef]
75. Brown, J.; Jorgenson, M.T.; Smith, O.P.; Lee, W. Long-term rates of erosion and carbon input, Elson Lagoon, Barrow, Alaska. In Proceedings of the 8th International Conference on Permafrost, Zürich, Switzerland, 21–25 July 2003; pp. 101–106.
76. Lantuit, H.; Overduin, P.P.; Couture, N.; Wetterich, S.; Are, F.; Atkinson, D.; Brown, J.; Cherkashov, G.; Drozdov, D.; Forbes, D.; et al. The Arctic Coastal Dynamics database: A new classification scheme and statistics on Arctic permafrost coastlines. *Estuaries Coasts* **2012**, *35*, 383–400. [CrossRef]

